



TECHNISCHE
UNIVERSITÄT
WIEN
Vienna University of Technology

D I P L O M A R B E I T

Combustion Structure of Nonpremixed, Coflowing Hydrocarbon Fuel Flames

ausgeführt zum Zwecke der Erlangung des Akademischen Grades eines
Diplom-Ingenieurs unter der Leitung von

Ao. Univ-Prof. Dipl.-Ing. Dr.techn. Ernst Pucher
E315 – Institut für Verbrennungskraftmaschinen und Kraftfahrzeugbau
Technische Universität Wien

Prof. Dr. Kalyanasundaram Seshadri
Department of Mechanical and Aerospace Engineering
University of California at San Diego, USA

eingereicht an der Technischen Universität Wien
Fakultät für Maschinenwesen und Betriebswirtschaften

von

Johannes Pitzl
Matrikelnummer: 0325586
Russengasse 12/5/17
3100 St.Pölten

Wien, Juli 2010

Combustion Structure of Nonpremixed, Coflowing Hydrocarbon Fuel Flames

Diploma Thesis

Johannes Pitzl

Institute of Internal Combustion Engines and Automotive
Engineering

Vienna University of Technology

Advisor:

Ao. Univ-Prof. Dipl.-Ing. Dr.techn. Ernst Pucher
Institute of Internal Combustion Engines and Automotive Engineering
Vienna University of Technology

Prof. Dr. Kalyanasundaram Seshadri
Department of Mechanical and Aerospace Engineering
University of California at San Diego, USA

San Diego, July 2010

Abstract

The rising costs of jet fuel coupled with an increased dependence on foreign crude oil has spawned a renewed interest in alternative fuels by the US Air Force. It is their goal to supply fifty percent of the continental U.S. Air Force with domestic sources by 2016.

This rejuvenated enthusiasm for alternative jet fuels has aroused the need for an improved understanding of the combustion of liquid hydrocarbons. Currently, there is a lack of empirical combustion data for controlled, liquid fueled laboratory flames such as the co-flow flame. To bridge this gap of limited knowledge, the Air Force runs Computational Fluid Dynamics (CFD), chemical kinetic model with chemistry and the University of California at San Diego (UCSD) provides them with experimental data of co-flow diffusion flames.

Jet Propellant 8 (JP-8) from crude oil is comprised of hundreds of different types of hydrocarbon compounds. With such a large variety of different components, different batches of JP-8 can lead to many different reactions during the burning process. To simulate these types of flames, it often takes significant amount of time because of the many reactions that can occur during combustion. To simplify the process, a much more simplified hydrocarbon mixture was developed such that the physical and combustion characteristics of the mixture appears similar to those of the commercial fuels. Such a mixture is called a surrogate fuel.

In the present study, JP-8, Fischer-Tropsch (FT) Shell GTL, and FT IPK Sasol fueled diffusion flames were compared to the flames fueled by the Aachen Surrogate, JP-8 Surrogate C, SERDP Surrogate, Modified SERDP Surrogate and Gasoline Surrogate C. The experiments were performed using the UCSD co-flow burner setup which is comprised of diffusion flame surrounded by a coaxial air flow. The main goal of this thesis was to measure flame heights for the different kerosene fuels as a function of fuel stream velocity and mass fraction.

The experimental studies demonstrate that the Aachen Surrogate, JP-8 Surrogate C, and SERDP Surrogate reproduce the flame height as a function of fuel stream velocity for FT Shell GTL and FT IPK Sasol very well. Additionally, the Aachen Surrogate, JP-8 Surrogate C, and SERDP Surrogate match with the lift-off height as function of fuel mass fraction for JP-8. It was also revealed that during flame lift-off there was a distinct match between JP-8, and JP-8 Surrogate C. To compare the empirical data with a numerical solution, the Burke-Schumann equation was used. Using this equation, experimental data matched with the trend of the calculated values for flame height.

Kurzfassung

Die steigenden Kosten für Flugzeugtreibstoff und die Erhöhung der Abhängigkeit von ausländischem Erdöl hat das Interesse der U.S. Air Force an alternativen Kraftstoffen erneut geweckt. Das ehrgeizige Ziel ist es fünfzig Prozent des kontinentalen U.S. Air Force Treibstoffbedarfs durch inländische Quellen bis 2016 zu decken.

Diese erneute Aufmerksamkeit für alternative Düsenkraftstoffe hat die Notwendigkeit für ein verbessertes Verständnis der Verbrennung von flüssigen Kohlenwasserstoffen aufgezeigt. Es besteht ein Mangel an Daten von kontrollierten Verbrennungen von flüssigen Kraftstoffen in Laborumgebung, wie es zum Beispiel die Diffusionsflamme im Coflow Burner Experiment darstellt. Um die Lücke fehlender Daten zu schließen arbeitet die U.S. Air Force mit Computational Fluid Dynamics (CFD) Simulationen mit chemischen Modellen und die University of California in San Diego (UCSD) stellt die experimentellen Daten von den Coflow Diffusionsflammen zur Verfügung.

Düsenkraftstoff 8 (Jet Propellant 8, JP-8) aus Rohöl ist ein Gemisch von Hunderten von Kohlenwasserstoffverbindungen und das verursacht eine enorme Vielfalt an unterschiedlichen Reaktionen während des Brennvorgangs. Computersimulationen für diese Art von Brennstoffe sind, aufgrund der Menge der Reaktionen bei der Verbrennung, mit langen Rechenzeiten verbunden. Daher werden Mischungen aus einigen wenigen Kohlenwasserstoffkomponenten entwickelt. Deren relative Konzentrationen kann so eingestellt werden, dass ihre physikalischen Eigenschaften und ihre Verbrennungseigenschaften die der kommerziellen Kraftstoffe abbilden. Diese Mischungen werden Ersatzkraftstoffe (Surrogates) genannt.

In der vorliegenden Studie wurden JP-8, Fischer-Tropsch (FT) Shell GTL und FT IPK Sasol Diffusionsflammen mit den Flammen von Aachen Surrogate, JP-8 Surrogate C, SERDP Surrogate, Modified SERDP Surrogate und Gasoline Surrogate C verglichen. Die Experimente wurden mit Hilfe des UCSD Coflow Burner Experiments, indem eine Diffusionsflamme umgeben von einem coaxialen Luftstrom erzeugt wird, durchgeführt. Das Hauptaugenmerk dieser Arbeit lag darin, bestehende Surrogates für Kerosin Kraftstoffe für die Tauglichkeit bei Diffusionsflammen, speziell für die Flammenhöhe bei konstantem Kraftstoffmassenanteil und veränderlicher Kraftstoffaustrittsgeschwindigkeit, zu bewerten. Flammen Lift-Off Höhen für konstante Kraftstoffaustrittsgeschwindigkeit als Funktion vom veränderlichen Kraftstoffmassenanteil bilden den zweiten Teil dieser Arbeit.

Diese experimentelle Studie zeigt, dass das Aachen Surrogate die Flammenhöhe als Funktion der Kraftstoffaustrittsgeschwindigkeit für FT Shell GTL und FT IPK Sasol sehr gut wieder gibt und dass das Aachen Surrogate mit der Flammen Lift-Off Höhe als Funktion des Kraftstoffmassenanteils für JP-8 korreliert. Für die Flammenhöhen während des Flammen Lift-Off Experiments wurde nur ein Trend zwischen JP-8, Aachen Surrogate und JP-8 Surrogate C gefunden. Das Diffusionsflammenproblem behandelt von Burke und Schumann stellt den numerischen Teil der Arbeit dar und wurde verwendet, um die experimentellen Daten zu evaluieren. Die Arbeit konnte zeigen, dass der Trend der Berechnung den Trend des Flammenhöhenexperiments widerspiegelt.

Acknowledgments

I would like to express my gratitude to all those who gave me the opportunity to write and complete this diploma thesis at the University of California at San Diego. First and foremost, I would like to extend a warm thank you to thank Prof. Dr. Ernst Pucher, my advisor at the Vienna University of Technology, who encouraged me to do my thesis abroad. His sustained effort to support students with his international relationships made this opportunity possible.

Furthermore, I am grateful to my advisor at the University of California San Diego, Prof. Dr. Kalyanasundaram Seshadri, who invited me to San Diego and supported me during my stay with his academic knowledge as well as in my daily life activities.

I want also to thank my co-workers in the lab, Ulrich Niemann and Tei Newman-Lehman. Their advice helped to develop the ideas for my thesis as well as what to do during my stay in San Diego.

And a special thanks should go to my girlfriend Elisabeth who helped me with my preparations for the stay in San Diego with love and comprehension. I am also thankful for my great family who made this stay as comfortable as it was.

Contents

List of Symbols	III
Subscript	IV
1. Introduction	1
1.1. Fuels	2
1.1.1. Kerosene	2
1.1.2. Fischer-Tropsch Kerosene	3
1.2. Surrogates	5
1.2.1. Aachen Surrogate	5
1.2.2. JP-8 Surrogate C	6
1.2.3. SERDP Surrogate	6
1.2.4. Modified SERDP Surrogate	7
1.2.5. Gasoline Surrogate C	7
1.3. Definition of Flames	9
1.3.1. Premixed Flame	9
1.3.2. Diffusion Flame	9
2. Experimental Setup	11
2.1. Experimental Apparatus Description	11
2.1.1. Burner Body	12
2.1.2. Vaporization System	16
2.1.3. Gas Handling System	17
2.1.4. Heating System	19
2.1.5. Temperature Control System	20
2.1.6. Plumbing System	21
2.1.7. Exhaust System	22
2.2. Data Acquisition	23
3. Experimental Procedure	25
3.1. Fuel Stream Velocity Calculation	25
3.2. Statistics	26
4. Experiments	28
4.1. Flame Height Experiments	28
4.2. Lift-Off Hysteresis Experiments	29
4.3. Diffusion Flame Problem by Burke-Schumann	30
5. Experimental Results	35
5.1. Flame Height Experiment	35
5.1.1. Flame Height Results of Fuels	36

5.1.2.	Flame Heights of Surrogates	37
5.1.3.	Conclusion of the Flame Height Experiment	38
5.2.	Lift-Off Hysteresis Experiment	39
5.2.1.	Lift-Off Hysteresis of Fuels	39
5.2.2.	Lift-Off Hysteresis of Surrogates	40
5.2.3.	Conclusion for Lift-Off Hysteresis Experiment	41
5.3.	Flame Height during Lift-Off Experiments	42
5.3.1.	Flame Height of Fuels during Lift-Off	42
5.3.2.	Flame Height of Surrogates during Lift-Off	43
5.3.3.	Conclusion of Flame Height during Lift-Off Experiment	43
5.4.	Burke-Schumann	44
5.4.1.	Flame Height for Diffusion Flame Problem by Burke-Schumann	46
5.4.2.	Conclusion of Flame Height for Diffusion Flame Problem by Burke-Schumann	48
6.	Concluding Remarks	50
	List of Figures	56
	List of Tables	57
A.		i
A.1.	Experimental Data for Flame Height Experiment	i
B.		x
B.1.	Experimental Data for Lift-Off Height Hysteresis Experiment	x

List of Symbols

a	Diameter of the fuel nozzle
A	Cross section
b	Inner tube diameter
c	Ratio between inner tube and diameter of the fuel nozzle
D	Diffusion coefficient
\bar{h}	Mean value
$J_0(\varphi)$	Bessel function of order 0
$J_1(\varphi)$	Bessel function of order 1
P	Probability
s	Standard deviation
\bar{s}	Standard deviation of the mean value
T	Temperature
v	Velocity
\dot{V}	Flow rate
W	Molecular weight
x_w	Truth value
\bar{x}	Mean value
Y	Mass fraction
z	Flame height
β	Coupling function
φ	Variable of the Bessel function
γ	Reduced variable for Burke-Schumann equation
η	Dimensionless coordinate of flame height
ν	Initial molar mixture strength
ν	Stoichiometric coefficient
ρ	Density
ξ	Dimensionless coordinate of horizontal position

Subscript

1	Fuel duct side
2	Oxidizer duct side
<i>air</i>	Air
<i>co – flow</i>	Coaxial flow
<i>f</i>	Flame
<i>F</i>	Fuel
<i>lift – off</i>	Lift-off
<i>nozzle</i>	Fuel nozzle
<i>N₂</i>	Nitrogen
<i>O₂</i>	Oxygen
<i>vapor</i>	Vaporizer

Chapter 1.

Introduction

The rising costs of jet fuel and the increasing reliability on foreign crude oil has renewed U.S. Air Force interests in alternative fuels. The U.S. Air Force has set a goal to supply fifty percent of its continental U.S. Air Force fuel requirements from domestic synthetic sources by 2016 and has been a major advocate of rapidly implementing alternative fuel technologies to supplement oil. This goal will be met by using blends of JP-8 and Fischer-Tropsch (FT) fuels, generated from natural gas and potentially other sources such as coal and biomass. However, this is a difficult task and in the near-term, it is desirable that the alternative fuels have similar combustion characteristics as JP-8.

The now renewed attention of alternative jet fuels has supported the need for an improved understanding of the combustion of liquid hydrocarbon fuels. Unfortunately, the lack of combustion data in controlled, liquid fueled laboratory flames, such as co-flow jet diffusion flames, is a major handicap to achieving an improved understanding.

Computational Fluid Dynamic (CFD) simulations with chemistry are used to aid the understanding and prediction of combustion processes. Validated simulations can also be used to investigate the combustion characteristics of alternative fuels with known chemical composition. The problem is that detailed kinetic models are required to compute properly flames burning complex fuels.

Detailed chemistry models are being developed for surrogate JP-8 and alternative fuels, however; the lack of fundamental data for laboratory flames has restrained the validation of the CFD codes with detailed chemistry. The proposed simulation/experimental program of the Air Force addresses the difficult problem of obtaining combustion data for JP-8 and alternate surrogate fuels in laboratory flames and using that data to validate detailed chemistry kinetic models.

As CFD simulation tool a Navier-Stokes based, 2D, time dependent simulation called

UNsteady Ignition and COMbustion with ReactionS (UNICORN) is used. This software evaluates detailed chemistry models for surrogate JP-8 and alternative fuels. Experimental data is needed to validate and evaluate the simulation results data of the different fuels.

Although several detailed fuel chemistry models have been developed but they have not been validated sufficiently because of the lack of experimental data of fundamental flames and the difficulty of evaluating large chemical mechanisms.

The importance of understanding laminar non premixed flames is used for plane and space ship propulsion as well as for small applications such as gas ovens, ranges and heating applications. With the current demand for large amounts of economical, clean power there is a need of research in decreasing the fuel consumption by increasing the combustion efficiency.

To study this laminar diffusion flames the team of Professor Kalyanasundaram Seshadri has built one of the first co-flow burners which can handle liquid fuel for the co-flow diffusion flame experiments. Before, most of the diffusion flame experiments were done only with gaseous fuels.

The attention in this thesis was to get experimental data for flame heights and lift off heights of three individual jet fuels and three individual surrogates at different conditions. The jet fuels used are crud oil JP-8, FT Shell GTL from a natural gas to liquid process, and FT IPK Sasol from a coal source. The surrogates used during the experiments are Aachen Surrogate, JP-8 Surrogate C, SERDP Surrogate, Modified SERDP Surrogate, and Gasoline Surrogate C. Also a numeric part was carried out to complete the thesis. This numeric part is called the Diffusion Flame Problem by Burke and Schumann. The calculations were made for all three jet fuels and the five surrogates as well as for the single components for the surrogates.

1.1. Fuels

1.1.1. Kerosene

Kerosene is a distillate fraction of crude oil with a boiling temperature between 420 K and 520 K . Its density is greater than naphtha and gasoline but less than diesel. Kerosene was one of the earliest petroleum products to be produced by refiners.

Kerosene used in aircrafts is called "aviation turbine fuel". In 2007, the consumption of aviation turbine fuel world wide was estimated at 205 million tons, and demand is growing at a faster rate than that of other petroleum products. Small volumes of kerosene are utilized for other needs such as illumination and cooking. [11]

The major difference between U.S. military fuels and commercial fuels is the use of certain additives, such as anti-icing, corrosion inhibitors, lubricity improvers, antioxidants, thermal stability improvers, conductivity improvers, and more. Usage of additives in civilian jet fuel is by agreement between user and supplier. JP-8 is the military equivalent of JET A-1, with the additives mentioned above. JP-8 is mainly used by the U.S. Air Force and meets the requirements of British specifications DEF STAN 91-87 AVTUR/FSII. [11]

1.1.1.1. JP-8

JP-8 is a very complex mixture of maybe thousands of species whose concentrations differ with different batches of fuel. Table 1.1 shows the properties of JP-8, FT Shell GTL, FT IPK Sasol, Aachen Surrogate, JP-8 Surrogate C, SERDP Surrogate, Modified SERDP Surrogate, and Gasoline Surrogate C.

Table 1.1.: Properties of Jet Fuels and Surrogates used during the Experiments

Fuel	Molecular Weight [g/mol]	Density [kg/m ³] @ 298 K	Melting Point [K]	Pyrolysis Point [K]
JP-8	147.83	803.6	222.2	643.2
FT Shell GTL	156.5	736.1	219.2	643.2
FT IPK Sasol	170.3	768.8	208.2	< 613.2
Aachen Surrogate	137.24	755.0	-	-
JP-8 Surrogate C	132.14	773.6	-	-
SERDP Surrogate	147.18	759.9	-	-
Modified SERDP Surrogate	145.62	771.0	-	-
Gasoline Surrogate C	103.27	743.2	-	-

1.1.2. Fischer-Tropsch Kerosene

Fischer-Tropsch technology was discovered in the early last century along with many other bulk chemical technologies. Its development has been hampered by the lack of a reliable commercial market. Interest in Fischer-Tropsch technology as a source of alternate fuel has been in spurts, driven by political situations and peaks in the price and availability of crude oil. There have been surges of interest in the thirties and during the Second World War, in the fifties, as a result of the oil crisis of the seventies and now again in the last

twelve years.

The qualities of Fischer-Tropsch products are excellent and their environmental properties are being recognized as very valuable in the ongoing drive towards cleaner fuels and engines. The beginnings of Fischer-Tropsch were in the search of for ways to turn coal into a liquid transport fuel, now it is likely for means of monetizing natural gas.

Gas to Liquids technologies, or GTL as it is referred to, is a complex integrated set of technology with Fischer-Tropsch at its heart. Today the commercial operations are in South Africa (both coal and natural gas) and Malaysia.

Fischer-Tropsch technology can be briefly explained as a means to convert synthesis gas containing hydrogen and carbon monoxide to hydrocarbon products. The hydrocarbon products are mostly liquid at ambient air but some are gaseous and some may even be solid. Interest in Fischer-Tropsch technology is increasing rapidly. This is due to recent improvements of the technology and the realization that it can be used to obtain value from stranded natural gas. Remotely located natural gas will be converted to liquid hydrocarbon products that can be sold in world wide markets.

The most popular application is to utilize abundant and low cost natural gas to produce 'clean', with low content of sulphur and aromatics, middle distillates/fuels, with the main co-product being a paraffinic naphtha. Some advantages of Fischer-Tropsch hydrocarbons compared to crude oil as a feedstock for fuel production are the absence of sulphur, nitrogen and heavy metal contaminates and the low aromatic content.

The so produced kerosene/jet fuel has good combustion properties, high smoke points and the diesel fuel with its high cetane number can be used to upgrade lower quality blend stocks produced from crude oil. [15]

1.1.2.1. FT Shell GTL

The company Shell derives their Fischer-Tropsch kerosene by the natural gas to liquid process. A low temperature cobalt catalyst is used by Shell for the production of their FT Shell GTL. The refinery process by Shell to convert FT kerosene from the intermediate product is based on hydrocracking, isomerization and fractionation [8].

Properties of FT Shell GTL can be seen in Table 1.1.

1.1.2.2. FT IPK Sasol

Sasol is a South African company involved in mining, energy, chemicals and synfuels. Sasol's primary business is based on coal to liquid (CTL) and GTL. The fuel used for the experiments in this thesis is a coal-derived kerosene by using a high temperature iron catalyst. In order to convert FT kerosene its intermediate product Sasol applies hydrogenation and fractionation [8].

Properties of FT IPK Sasol are shown in Table 1.1.

1.2. Surrogates

Due to the wide variety of different chemical reactions in the burning process of fuels, numerical calculations of combustion is challenging. Practical fuels for example, gasoline, diesel and jet fuels contain hundreds of aliphatic and aromatic hydrocarbon compounds. The major components of jet fuels are straight chain paraffins, branched chain paraffins, cyclo-paraffins, aromatics and alkenes [5]. Surrogate fuels are defined mixtures of few hydrocarbon compounds with combustion characteristics similar to those of commercial fuels [4]. The concentrations of surrogates can be adjusted so that the physical and chemical properties pertinent to combustion approximate those of commercial fuels [12].

The “reference” fuels used as components for the surrogates of jet fuels are n-heptane, n-decane, n-dodecane, iso-octane, methylcyclohexane, toluene, trimethylbenzene, m-xylene, and o-xylene. Five surrogates are tested during this here. They are Aachen Surrogate, JP-8 Surrogate C, SERDP Surrogate, Modified SERDP Surrogate, and Gasoline Surrogate C. The properties of these surrogate fuels are given in Table 1.1.

Surrogate fuels are important for understanding fundamental-combustion processes and for evaluating fuel chemistry models.

1.2.1. Aachen Surrogate

The Aachen Surrogate is made up of 80 % n-decane, and 20 % trimethylbenzene by weight as seen in Table 1.2 and the properties of its single components are given in Table 1.7 below. This surrogate reproduces the combustion characteristics of petroleum-derived JP-8 in the counter flow burner experiment best [1].

Table 1.2.: Aachen Surrogate composition and properties of employed components

Fuel	Chemical Symbol	Vol% @298K	Weight%	Mol%	Molecular Weight [g/mol]	Density [kg/m ³] @298K
n-Decane	C ₁₀ H ₂₂	82.8	80	73.8	142.28	730.0
Trimethyl- benzene	C ₉ H ₁₂	17.2	20	26.2	120.19	876.0

1.2.2. JP-8 Surrogate C

The JP-8 Surrogate C (UCSD Surrogate) is made up of 60 % n-dodecane, 20 % methylcyclohexane, and 20 % o-xylene by liquid volume. The composition of JP-8 Surrogate C can be seen in Table 1.3 and the properties of its single components are given in Table 1.7. This surrogate was developed at UCSD and reproduces best extinction and autoignition characteristics of JP-8 [6].

Table 1.3.: JP-8 Surrogate C composition and properties of employed components

Fuel	Chemical Symbol	Vol% @298K	Weight%	Mol%	Molecular Weight [g/mol]	Density [kg/m ³] @298K
n-Dodecane	C ₁₂ H ₂₆	60	56.6	43.9	170.33	730.0
Methylcyclo- hexane	C ₇ H ₁₄	20	20.6	27.8	98.21	798.0
o-Xylene	C ₈ H ₁₀	20	22.8	28.3	106.17	880.0

1.2.3. SERDP Surrogate

The SERDP Surrogate is made up of 77 % n-dodecane, and 23 % m-xylene by molar volume. The composition of the SERDP Surrogate is shown in Table 1.4 and the properties of its single components are given in Table 1.7.

Table 1.4.: SERDP Surrogate composition and properties of employed components

Fuel	Chemical Symbol	Vol% @298K	Weight%	Mol%	Molecular Weight [g/mol]	Density [kg/m ³] @298K
n-Dodecane	C ₁₂ H ₂₆	86.36	84.3	77	170.33	730.0
m-Xylene	C ₈ H ₁₀	13.64	15.7	23	106.17	860.0

1.2.4. Modified SERDP Surrogate

The Modified SERDP Surrogate is made up of 80 % n-dodecane, and 20 % toluene by weight. The composition of Modified SERDP Surrogate is given in Table 1.5 and the properties of its single components are shown in Table 1.7.

Table 1.5.: Modified SERDP Surrogate composition and properties of employed components

Fuel	Chemical Symbol	Vol% @298K	Weight%	Mol%	Molecular Weight [g/mol]	Density [kg/m ³] @298K
n-Dodecane	C ₁₂ H ₂₆	82.2	80	68.4	170.3348	730.0
Toluene	C ₇ H ₈	17.8	20	31.6	92.1384	866.9




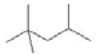

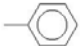
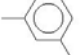
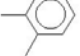
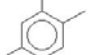
1.2.5. Gasoline Surrogate C

The Gasoline Surrogate C is made up of 20 % n-heptane, 40 % iso-octane, 20 % toluene, and 30 % methylcyclohexane by liquid volume. This surrogate was designed and developed to reproduce the combustion characteristics of gasoline best. The composition of the Gasoline Surrogate C can be seen in Table 1.6 and the properties of its single components are given in Table 1.7 [1].

Table 1.6.: Gasoline Surrogate C composition and properties of employed components

Fuel	Chemical Symbol	Vol% @298K	Weight%	Mol%	Molecular Weight [g/mol]	Density [kg/m ³] @298K
n-Heptane	C ₇ H ₁₆	20	18.4	19.0	100.2019	684.0
iso-Octane	C ₈ H ₁₈	40	37.8	34.2	114.2285	720.0
Toluene	C ₇ H ₈	10	11.6	13.0	92.1384	862.0
Methylcyclo- hexane	C ₇ H ₁₄	30	32.2	33.9	98.1861	798.0

Table 1.7.: Properties of all single surrogate components in detail [9] [18].

Name	Chemical Structure	Melting Point [K]	Boiling Point [K]	Flash Temp. [K]	Autoign. Temp. [K]
n-Heptane		182.6	371.5	269.2	558.2
n-Decane		245.3	446.9	319.1	483.2
n-Dodecane		263.5	489.0	347.1	476.1
iso-Octane		166.0	372.0	268.7	690.2
Methylcyclohexane		146.5	374.2	267.2	531.2
Toluene		180.2	383.8	277.2	753.2
m-Xylene		225	412	298.2	800.2
o-Xylene		248	417	305.2	736.2
Trimethylbenzene		227.0	442.4	317.1	773.1

1.3. Definition of Flames

1.3.1. Premixed Flame

In premixed combustion the oxidizer is mixed with the fuel at a molecular level before it reaches the reaction zone of flame front. This creates a thin flame as all reactants are readily available. If the mixture is rich, a diffusion flame will be generally found farther downstream.

If the flow of the fuel–oxidizer mixture is laminar, the flame speed of premixed flames is dominated by the chemistry. If the flow rate is below the flame speed, the flame will move upstream until the fuel is consumed, for example a Bunsen burner [20].

1.3.2. Diffusion Flame

In nonpremixed combustion mixing of oxidizer and fuel take place by diffusion. Combustion in this case is limited by the rate of diffusion, so the mixing of air and fuel controls the burning rate. Most particular systems fall into this category, and they are so-called diffusion flames in which fuel and oxidant come together in a reaction zone through molecular and turbulent diffusion. The fuel jet may be in form of a gaseous fuel jet or of a condensed phase (liquid or solid). The distinctive characteristic of a diffusion flame is that the burning rate is determined by the rate at which the fuel and oxidizer are brought together for reactions in proper proportions. Between the extremes in which the chemical reaction rate on the one hand and the mixing on the other hand control the burning rate, there is the region in which the chemistry and mixing have similar rates and must be considered together [3]. Diffusion flames tend to have a lower burning rate than premixed flames. Diffusion flames are depending on the diffusion rate of fuel and oxidizer and the premixed flames are depending on the chemical reaction rate which is faster than diffusion. Also diffusion flames produce more soot because there are not sufficient oxidizers in the flame to complete the reaction. An example for a diffusion flame is a candle.

In the combustion field, gaseous diffusion flames have received less attention than premixed flames, despite the fact that diffusion flames have greater practical application and are used more frequently [3].

The shape of a laminar jet of fuel depends only on the mixture fraction of fuel and oxidizer, i.e. the quantity of air supplied. If an excess of air is present the flame appears as closed and elongated. Such flames occur when a jet of fuel is exposed into a large volume of quiescent air, or when two coaxial jets are used, as in this thesis. If the air supply in the outer tube is reduced below an initial mixture strength of stoichiometric, a fan-shaped under-ventilated flame is produced as shown in 1.1.

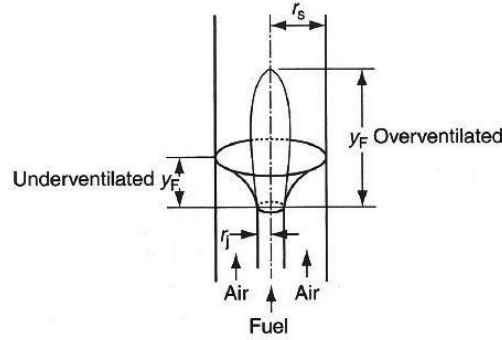


Figure 1.1.: The appearance of gaseous fuel jet flames [3].

This figure shows the coaxial co-flow of air (oxidizer) and fuel. The coordinate system in this figure is set up such that air and fuel flow in positive y -axis direction. Air and fuel are the flows of oxidizer and fuel, y_F is the flame height of the unerventilated or overventilated flame, r_s is the radius of the outer duct, and r_j is the nozzle radius.

Unlike the flame of premixed gases, which has a very narrow reaction zone with nearly constant element mass fraction, the diffusion flame has a wide horizontal region over which the element mass fraction changes. These changes are principally due to the interdiffusion of reactants and products since the actual reaction apparently takes place in a narrow zone. Hottel and Hawthorne (1949) measured the distribution of species through a laminar H_2 -air diffusion flame. The type of results they obtained for a radial distribution that would correspond to the broken line on Fig.1.1 is shown in Fig. 1.2

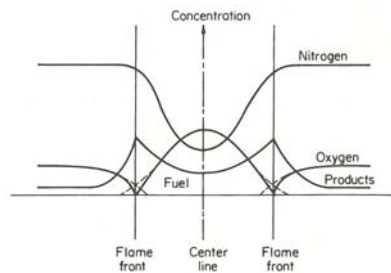


Figure 1.2.: Species variation through a diffusion flame at a fixed height above the fuel jet tube [3]

Figure 1.2 shows the center line of the flame as a vertical dashed line and the flame front as solid vertical lines on the left and right of the center line. The horizontal solid line is the zero level for reactant species concentrations at a specific height from the nozzle tip through the flame.

Chapter 2.

Experimental Setup

2.1. Experimental Apparatus Description

A stable, axi-symmetric flame is produced inside an apparatus herein referred to as a co-flow burner. In this burner configuration, separate mixtures of pre-heated air and fuel are routed through a network of heated pipes to the burner body where a series of separate meshes straighten the two flows that converge at the end of a stainless steel nozzle. There are several peripheral subsystems referred to in this thesis as the vaporization, gas handling, heating, temperature control, plumbing, flow control and exhaust system, needed for the proper operation of the experiment.

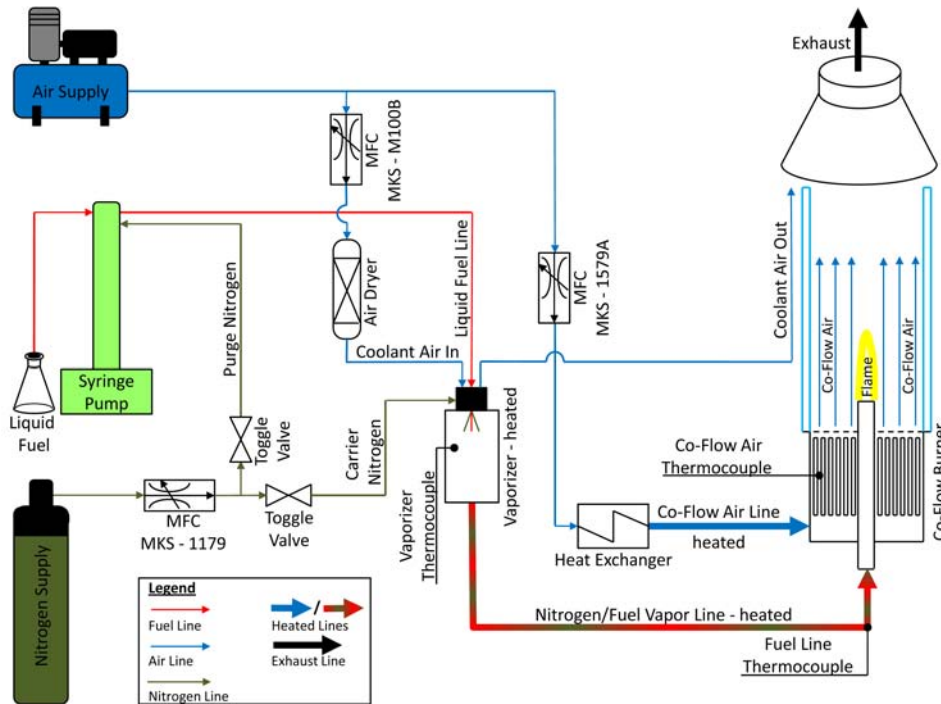


Figure 2.1.: Schematic illustration of the experimental setup. The figure shows the co-flow burner, the vaporizer and the air, fuel and nitrogen feed system.

The experimental setup as seen in Figure 2.1 consists of the co-flow burner itself, the heated vaporizer, the air, fuel and nitrogen supply and the measuring and controlling equipment.

In Figure 2.2 the control and measurement equipment is shown schematically. The control and measurement setup consists of PID controllers, solid state relays, K-Type thermocouples, heating tapes, mass flow controllers, a syringe pump, an ultrasonic nozzle, an ultrasonic broadband generator and a mass flow controller/power supply unit.

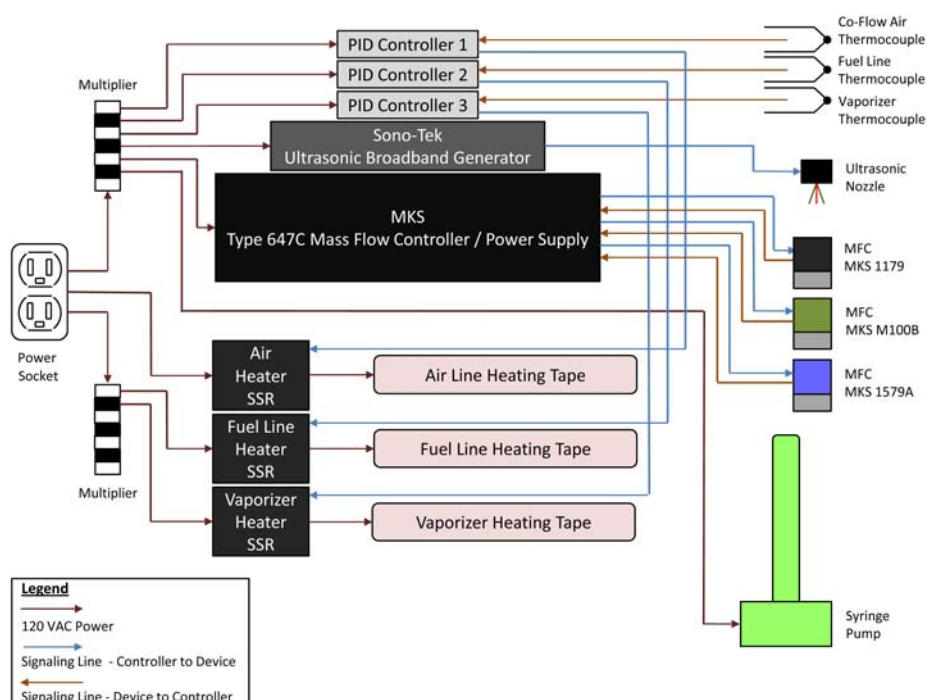


Figure 2.2.: Schematic illustration of the control and measurement setup and the wiring of the experimental setup.

2.1.1. Burner Body

The burner body (Figure 2.3-5) is the center piece of the experimental setup. Here a mixture of vaporized fuel and nitrogen come in contact with co-flow air. The burner body consists of several parts. These parts will be referred to as the bottom, air diffuser, tube holder, glass adapter, glass tube, fuel injector and nozzle piece.

The bottom piece is machined out of an aluminum cylinder 127 mm in diameter. It is sealed at the top end and pocketed on the other end to form a hollow toroid with an outside diameter of 110 mm and internal diameter of 27.5 mm. The center of this hollowed

cylinder has a 20 mm hole where the fuel injector section can enter through. Preheated air enters the bottom section tangentially through a pipe thread. On the periphery of the bottom are four bolt holes to secure a stand to the burner body which is further attached to an optical table.

The diffuser section is also machined out of an aluminum cylinder 60 mm long. This piece has an outer lip made by machining a 40 mm deep pocket alongside the outer edge. A pipe thread is cut into the center so that the fuel injector piece could be secured from the bottom. On the cylinder face opposite the peripheral lip is a centrally located pipe tap that is used to fasten either a nozzle or a nozzle adapter section. Since the pocketed lip removes a good deal of material from the edge of the cylinder, a thicker, centrally located aluminum section remains which consists 300 small, 2.55 mm holes equally spaced apart in a radial pattern. These holes act as the first stage to straighten and redirect the airflow as it moves its way from the inlet on the bottom section.

Bolted to the lip of the air diffuser section is the top section. The top section contains the meshes and the retaining rings that straighten the air flow. The top section is also machined out of an aluminum tube with an outer diameter of 127 mm and an inner diameter of 104.6 mm. It is designed such that the top half of the air diffuser section can slide up into the bottom half of the top section with a snug fit. To hold the meshes and retaining rings that are found inside, the bottom half of the top section has a 110 mm bore running 50mm down the length of the aluminum tube. To hold it to the rest of the burner body, there are six threaded holes machined in the same pattern as the through holes on the air diffuser and bottom section.

On top of the tube holder section the glass adapter piece is mounted. This piece forms the interface between the aluminum burner body and the Pyrex® glass section. It is also machined from an aluminum tube. It is designed such that the inside of the adapter slides on top of the outside of the top piece and the upper inside 20 mm of this adapter are machined to allow a tight fit between the aluminum and the glass interfaces.

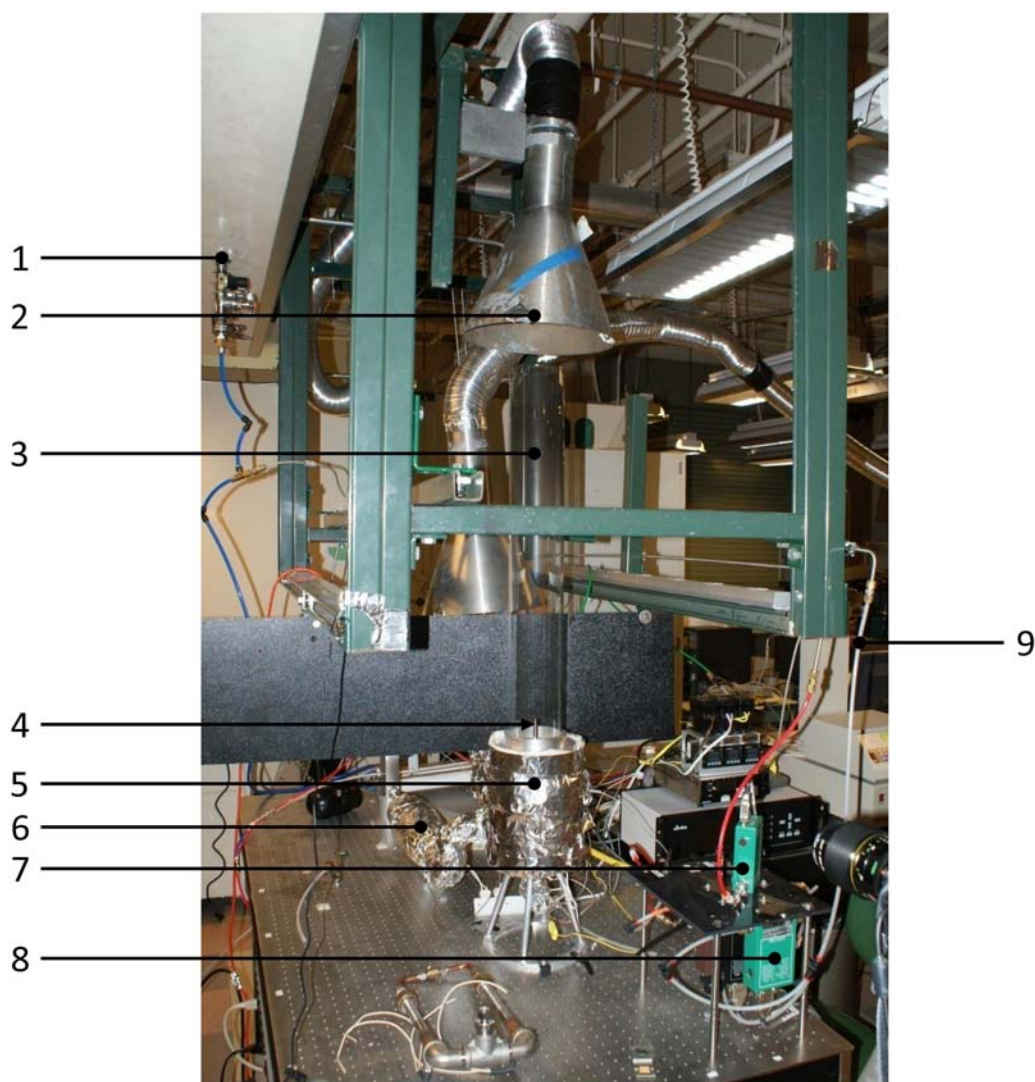


Figure 2.3.: The experimental setup: 1, In-house air supply; 2, Exhaust system; 3, Pyrex glass tube; 4, Fuel nozzle; 5, Burner body; 6, Custom built co-flow air heat exchanger; 7, Nitrogen mass flow controller; 8, Cooling air mass flow controller; 9, Cooling air supply.

Sitting on the top of the glass adapter section is the *Pyrex® glass tube* (Figure 2.3-3) itself. The glass tube can be one of three separate designs, specifically built to accomplish different experimental tasks. This includes taking gas chromatograph or temperature samples from any part of the flame. In the gas chromatograph sample design, a slot is cut into the center of the Pyrex® glass tube 55mm wide and 120 mm long. For temperature probe design, two holes are machined into the glass tube spaced 90 degree apart at a height that coincides with the nozzle opening. The second also serves as the opening for a very narrow, high voltage wire that can be used as an electrode to automatically relight the flame.

Threaded into the bottom of these three sandwiched sections (burner body, air diffuser section, and top section) is the fuel injector. This machined piece of stainless steel forms the junction between the fuel delivery system and the burner body. On top of it there is a separate stainless steel cone welded with six 1 mm holes drilled through it every 60 degrees. The complete assembly is threaded up into the air diffuser section so that during operation the nitrogen/fuel mixture can be routed through the nozzle.

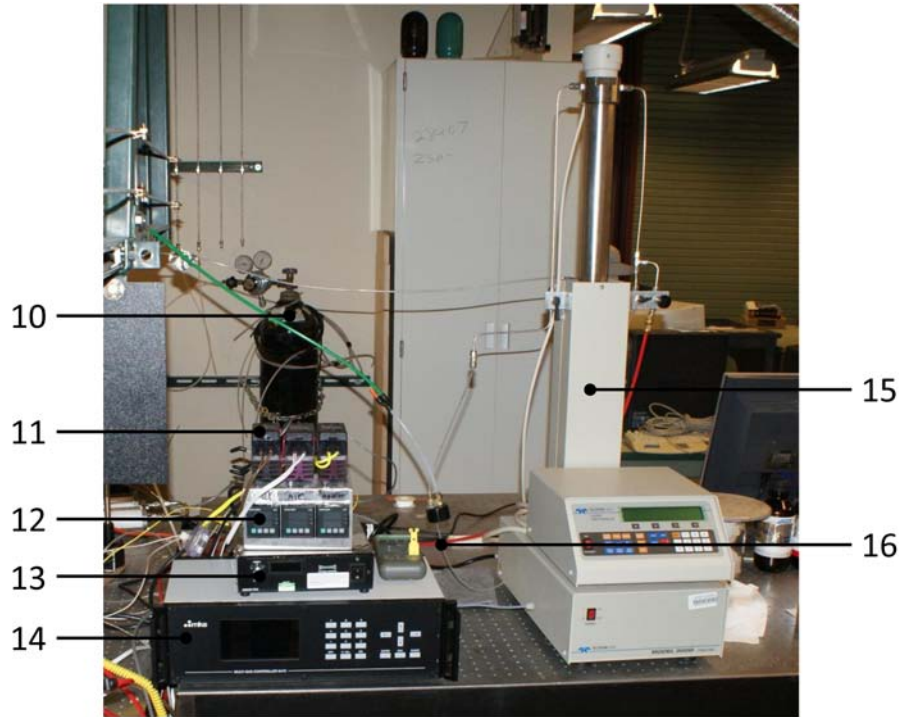


Figure 2.4.: The experimental setup: 10, Nitrogen gas cylinder; 11, Solid stage relays; 12, Watlow PID temperature controllers; 13, Ultra sonic broadband generator; 14, MKS mass flow controller power supply and control unit; 15, Syringe pump; 16, Fuel supply.

The hollow center of air diffuser section holds the nitrogen/fuel mixture that arrives from the fuel injector. A thread, located in the middle of the air diffuser section, is specifically designed to accommodate the fuel nozzle (Figure 2.3-4) or an adapter that can be used for smaller nozzle diameters. For most experiments it is desirable to have a smaller diameter fuel nozzle. During the experiments for this thesis a nozzle with a diameter of 6.1 mm was used. The nozzle rises approximately 115 mm above the top face of the air diffuser section. In order to maximize the laminar characteristics of the flow out of the nozzle, small nozzle meshes were installed at the nozzle tip. This was accomplished by carefully machining the nozzle out of two separate stainless steel pieces.

2.1.2. Vaporization System

In the vaporizer system the fuel vapor stream is generated by atomizing the liquid fuel with an ultrasonic nozzle and then mixing it with a varying amount of nitrogen. The Sono-Tek AccuMist™ Nozzle (Figure 2.7-20) used in this experiment generates a fuel mist with a mean size of 15 microns by a 120 kHz sound wave. This nozzle is threaded to the top part of the aluminum vaporizer and held in place with high temperature silicon.

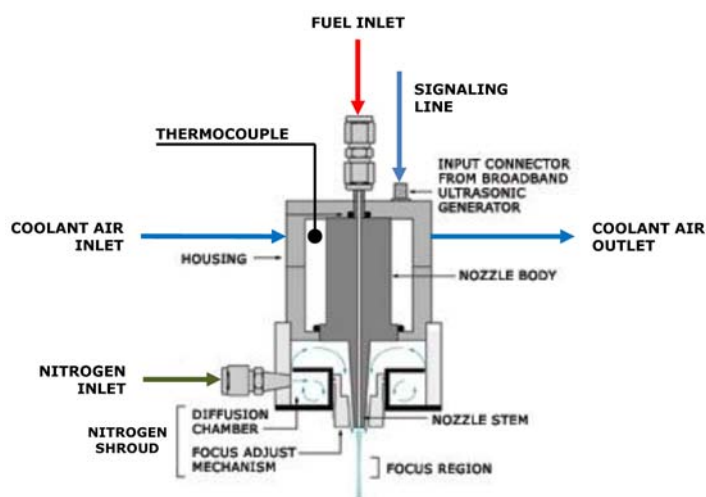


Figure 2.5.: Sectional view of a Sono-Tek AccuMist™ Nozzle with the specific experimental setting [13].

Figure 2.5 shows a cross section view of the Sono-Tek AccuMist™ Nozzle with the main parts and connectors. Fuel from the syringe pump reaches the nozzle on the top. There are two connectors for cooling air inlet and outlet at the housing. The nitrogen is going through the connector at the lower section into the diffusion chamber to the spray adjustment mechanism. With the help of this mechanism one can focus region of the fuel nitrogen spray.

Fuel is supplied by a Teledyne Isco Model 500D syringe pump with 500 ml fuel storage capacity and a flow rate that can vary between 0.001 ml/min and 250 ml/min.



Figure 2.6.: The Teledyne Isco Model 500D syringe pump [16].

The vaporizer body (Figure 2.12-29) consists of an aluminum tube with an outer diameter of 76.2 mm (3 in) and an inner diameter of 63.5 mm (2.5 in). It is 254 mm (10 in) long and welded shut at the bottom. A 1/4-national pipe thread (NPT) female pipe thread is machined into the bottom. This allows an easy attachment of the fuel delivery line. A stand attached to the vaporizer body holds the assembly onto the laser table. To heat the vaporizer, a heating tape is wrapped around the periphery of the aluminum tube and insulated with 1in layer of Insulfrax insulation (Figure 2.7-17).

2.1.3. Gas Handling System

To burn vaporized fuel in a controlled environment, it is necessary to maintain properly metered gas flows at all times. This is accomplished by using a wide variety of tubing, manual and automatic valves along with two digital control systems, as seen in Figure 2.1. Two gases are used, nitrogen and air. Gas cylinders supply the nitrogen (Figure 2.4-10) while an overhead air compressor (Figure 2.3-1) supplies air. Vaporized fuel is produced by means of the ultrasonic nozzle (Figure 2.5) connected to a chamber consisting of a large, heated aluminum tube. It is carried through heated, 6.35 mm (1/4 in) tubing (Figure 2.7-21) to the burner after being mixed with nitrogen.

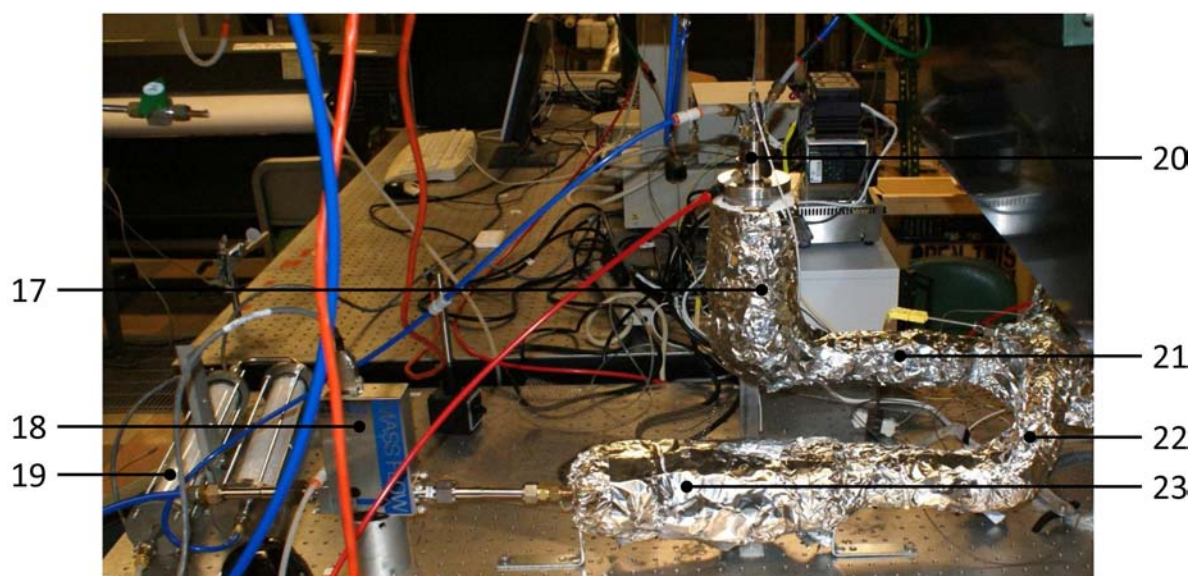


Figure 2.7.: The experimental setup: 17, Vaporizer with insulation; 18, Co-flow air mass flow controller; 19, Cooling air dryer; 20, Ultra sonic nozzle; 21, Heated fuel line with insulation; 22, Heated co-flow air line with insulation; 23, Custom built co-flow air heat exchanger.

Nitrogen flows from a gas cylinder regulator at 5.52 bar (80 psi) and is carried to a MKS 1179 mass flow controller (Figure 2.3-7) through a series of overhead plumbing. This mass flow controller accurately controls up to 200 standard cubic centimeters per minute (sccm) of nitrogen with an accuracy of ± 0.1 sccm. After being metered by the mass flow controller, the mass flow is split and sent to two Swagelok® toggle valves. These valves determine the destination of the flow to either vaporizer, where it acts as a carrier gas for the fuel or to the syringe pump where it can purge the fuel line of all remaining fuel when the experiment is concluded.



Figure 2.8.: MKS 1179, MKS 1579A, and MKS M100B mass flow controller [7].

The air supply comes from the in-house compressor system at 6.89 bar (100 psi). First, the flow is divided between the co-flow air stream and the ultrasonic nozzle cooling (Figure

2.3-9) system. The co-flow air stream is directed to a MKS 1579A mass flow controller which can provide up to 300 standard liters per minute (slm) with an accuracy of $\pm 1\%$ of full scale. From the mass flow controller, it is directed to the air heat exchanger and then to the burner body. Meanwhile, the ultrasonic nozzle cooling air is routed to an MKS M100B mass flow controller (Figure 2.3-8) rated to 50 slm. From there it is directed to a calcium sulfate drying apparatus (Figure 2.7-19) and then to the ultrasonic nozzle (Figure 2.12-24) where it serves to keep the nozzle at safe temperature.

2.1.4. Heating System

Since liquid fuel has the potential to condensate at room temperature, it is necessary to heat the incoming air, burner body, vaporizer and fuel delivery lines to high temperatures. This is done with the help of several heating tapes from Omega Instruments. Each heating tape measures 914.4 mm (3 feet) in length and is rated for up to 500 W at 120 VAC. Heating tapes are wired according to their placement in the experiment. The current version has three heating subsystems the co-flow air, fuel line, and vaporizer system.



Figure 2.9.: Omega Instruments Heating Tape [10].

Before entering the burner body, the co-flow air is preheated by means of a custom-built heat exchanger (Figure 2.7-23). This device is made from 304.8 mm (12 in) of 38.1 mm (1.5 in) copper tube silver soldered shut on both ends and filled with copper pellets. Two holes are drilled on each end to accommodate the copper tubing and then silver soldered in place. The co-flow air exits the heat exchanger and makes its way through the copper tubing where it enters the burner body. One heating tape is wrapped around the copper line and the other is placed around the burner body. All of these devices are wrapped with Insulfrax® insulation to minimize any unnecessary heat loss. These three heating tapes are connected in parallel to a standard female household multiplier.

The vaporizer is heated by one heating tape (Figure 2.12-26) wrapped around the outside and covered with Insulfrax® insulation. This heating tape is not connected to any others since the vaporizer is relatively small and the temperature is very important.

It is also necessary to heat up the fuel delivery line to ensure that vaporized fuel has a minimal condensation as it makes its way to the burner body. To ensure this, two heating tapes are wrapped around the entire length of the fuel line and wrapped with more Insulfrax® insulation. These two heating tapes are connected in parallel to another standard female household multiplier.

2.1.5. Temperature Control System

Temperature value and stability are critical factors in the success of this experiment. To ensure adequate temperature it is necessary to use closed loop proportional–integral–derivative (PID) control for the six different heating tapes in the experiment. With the three heating subsystems, thermocouples were placed in three strategic locations to accurately measure the process variable for each site. A separate Watlow Series 93 temperature controller adjusts each subsystem. These controllers measure the process variable and control it by applying an appropriate duty cycle regardless of gas and fuel flow rates.



Figure 2.10.: Watlow Series 93 PID temperature controller [19].

The temperature inside the vaporizer is measured with a specially designed Omega, K-Type thermocouple with a 1/8-NPT male pipe fitting. When the vaporizer was designed, an extra boss was welded onto a small part of the aluminum and threaded to accommodate the same 1/8-NPT thread. The wiring is routed to the Watlow PID temperature controller (Figure 2.4-12) which uses the information to determine the duty cycle for the heating tape. The proper duty cycle is turned into a low current DC square and sent to the Watlow DIN-A-MITE solid state relay (Figure 2.4-11) which adjusts the duty cycle of the household current to the vaporizer heating tape.

Temperature inside the fuel line is sampled directly before the fuel line ascend into the burner body by means of a K-Type thermocouple with a 3.175 mm (1/8 in) probe diameter using a Swagelok® pipe to tube adapter. Using the same approach as the vaporizer, this thermocouple data is sent to another dedicated Series 93 controller and DIN-A-MITE adjusts the duty cycle of the household current to the two fuel line heating tapes.

Air temperature is controlled by taking the process variable inside the burner body immediately before the co-flow air stream is mixed with the fuel stream. A 1/8-NPT female thread was machined into the burner body and another Omega K-type thermocouple installed. These data is sent directly to another dedicated Watlow controller where it sends the desired duty cycle to the DIN-A-MITE for optional temperature regulation.



Figure 2.11.: Omega® Thermocouple K-Type [10].

2.1.6. Plumbing System

A wide variety of tubing, quick fittings and Swagelok® fittings are used to ensure that the gases are routed to their proper destinations with minimal leakage.

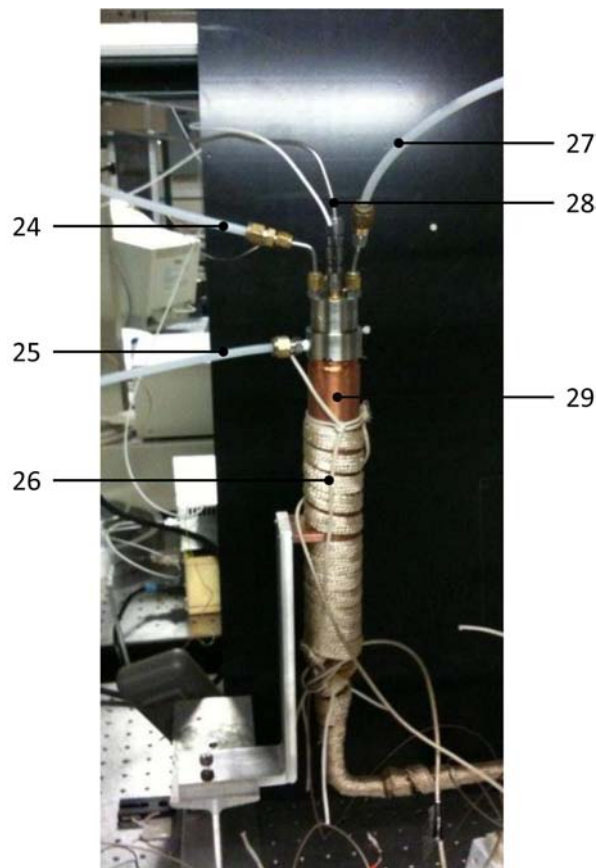


Figure 2.12.: The experimental setup: 24, Cooling air intake; 25, Nitrogen carrier gas intake; 26, Heating tape; 27, Cooling air outlet; 28, Fuel intake; 29, Vaporizer.

In house air comes from a Swagelok® fitting on the ceiling. This fitting attaches to a 6.35 mm (1/4 in) polyethylene tube that is split with a quick connect tee and send to the MKS 1579A mass flow controller and the MKS M100B mass flow controller with two pieces of 6.35 mm (1/4 in) polyethylene tubing. These tubes are both connected to the mass flow controllers via quick connect unions. After the MKS 1579A mass flow controller, the air is sent to the air heat exchanger where it leaves as a hot stream through a 9.525 mm (3/8 in) heated, copper delivery line (Figure 2.7-22). The air delivery line connects to a 9.525 mm (3/8 in) by 1/2-NPT Swagelok® pipe adapter that interfaces to the burner body. After the MKS M100B mass flow controller, air is routed to the cooling port entry (Figure 2.12-24) of the ultrasonic nozzle and it leaves through the cooling port exit (Figure 2.12-27) on the opposite side of the cooling air entry. Nitrogen is fed to the experiment from a gas cylinder through a 6.35 mm (1/4 in) stainless steel line close. Here, it is attached to a Swagelok® union that changes the tubing material from stainless steel to polyethylene. The plastic tubing makes its way to the MKA 1179 mass flow controller where it exits and is split with a quick connect tee where the two flows are sent to the toggle valves. When the two flows exit the built-in Swagelok® connectors on the toggle valves, the purge line is routed towards the syringe pump's built-in Swagelok® fitting while the fuel carrier line (Figure 2.12-25) is routed towards the fitting on the ultrasonic nozzle (Figure 2.5).

Liquid fuel is pumped through a 3.175 mm (1/8 in) polyethylene line from the syringe pump (Figure 2.4-15) to the ultrasonic nozzle (Figure 2.12-28) where it is attached with a 3.175 mm (1/8 in) Swagelok® connector. When the gaseous nitrogen/fuel mixture is formed it is routed away from the vaporizer through 6.35 mm (1/4 in) head brass tubing where it connects to the fuel injector so that it can make its progression up through the burner body and out the nozzle.

2.1.7. Exhaust System

A slight vacuum sucks the combustion gases and the ultrasonic nozzle cooling air on top of the Pyrex® glass tube out without influencing the combustion zone (Figure 2.3-2).

2.2. Data Acquisition

A digital single-lens reflex (DSLR) camera was used to capture data for the flame height and lift off height experiments. The DSLR camera was a Canon EOS D30 with a Canon macro lens FD100mm 1:4. The distance from the flame axis to the camera was 1270 mm (50 in) for the flame height experiments and 1855 mm (73 in) for the lift off hysteresis experiments as seen in Figure 2.13. This two different distances were necessary to get a superior resolution for the whole flame.

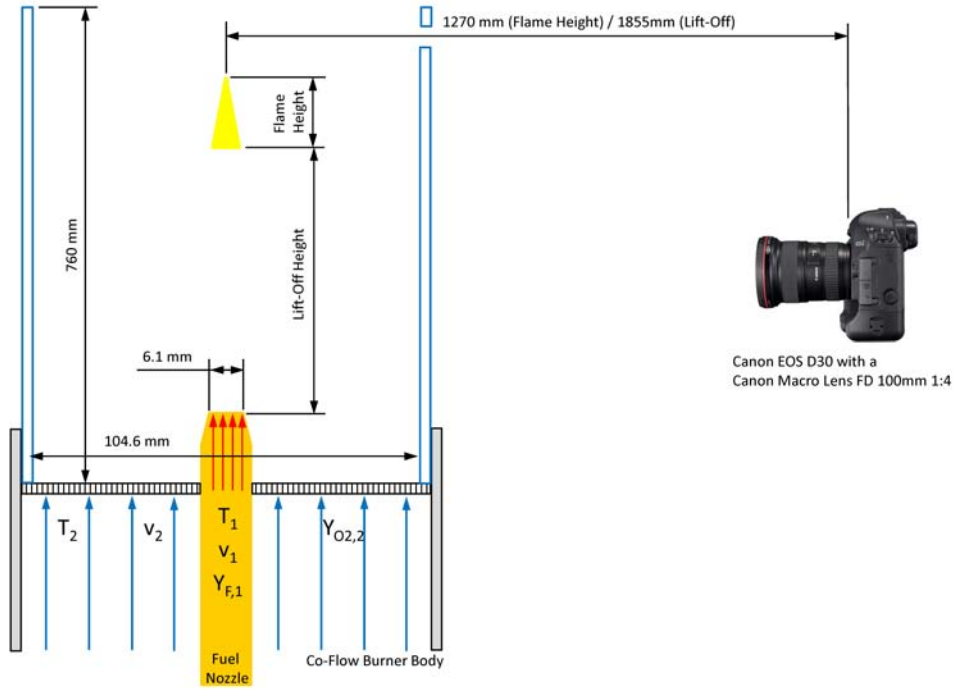


Figure 2.13.: Placement of the DSLR camera with macro lens for data acquisition. T_1 and T_2 are the temperatures of the fuel and the oxidizer duct, v_1 and v_2 are the velocities of the fuel stream and the oxidizer stream, $Y_{F,1}$ and $Y_{O2,2}$ are the mass fractions of fuel and oxygen.

To measure the flame height and the lift off height a licensed version of Adobe Photoshop CS3 was used. The diameter of the nozzle is a known value so one can calculate the real flame height or lift off height using this diameter with the pixels measured in Adobe Photoshop CS3 by using Equation 2.1 below.

$$z_f = \frac{a \cdot pixel_{flame\ height}}{pixel_{nozzle}} \quad (2.1)$$

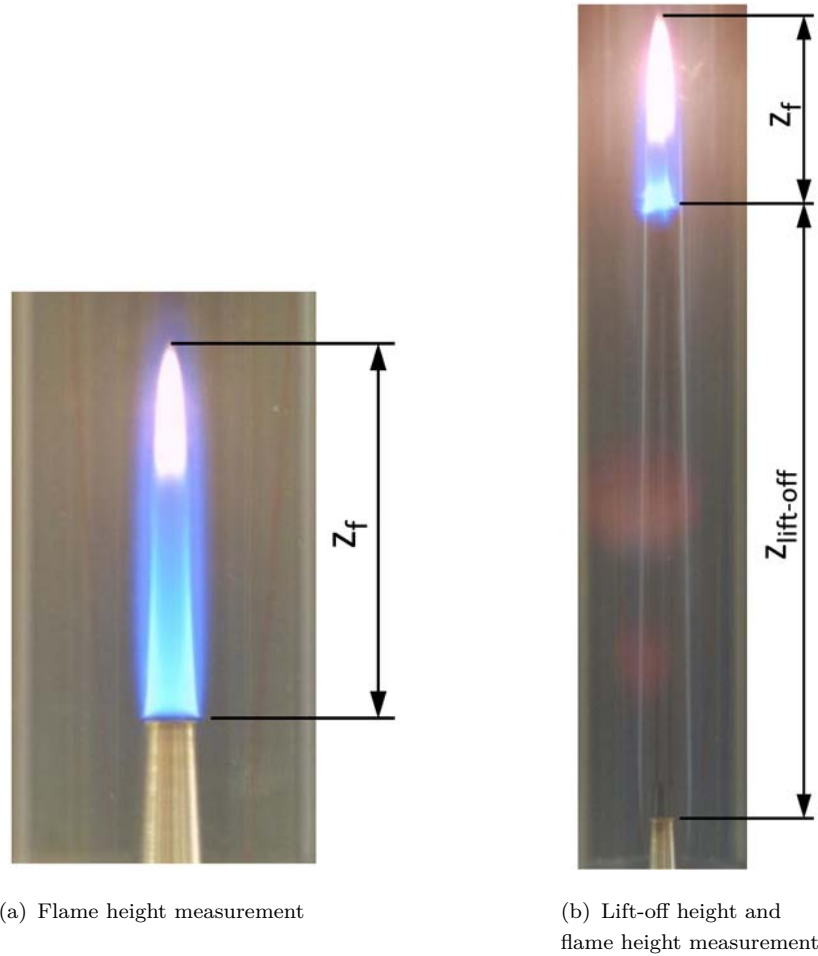


Figure 2.14.: Definition of the height measurements during the tests.

Figure 2.14(a) and Figure 2.14(b) show the definition of the flame height and lift-off height measurement during the experiments in this thesis. The flame height is measured from the bottom of the flame through the tip of the flame including the soot area and the lift-off height is measured from the tip of the fuel nozzle through the bottom of the lifted flame.

Chapter 3.

Experimental Procedure

3.1. Fuel Stream Velocity Calculation

The purpose of this experiment was to determine the heights of a flame with a constant fuel mass fraction but with different fuel exit velocities and constant co-flow air speed. Air velocity was determined using the the flow rate of compressed air as measured by the flow meter. Meanwhile, fuel stream velocity was determined by computing the total molar flow rate through the nozzle. Airflow velocity was determined by using the following equation,

$$v_2 = \frac{\dot{V}_{air,2} \cdot T_2 \cdot 1000}{273 \cdot 60 \cdot A_{co-flow}} \quad (3.1)$$

where the variable v_2 is the air velocity in cm/s that flows parallel to the fuel nozzle. T_2 represents the temperature of the oxidizer duct side in Kelvin and $A_{co-flow}$ is the effective cross section of the inner Pyrex® tube minus nozzle cross section in cm^2 . Here $A_{co-flow}$ is 86.19 cm^2 .

$$v_1 = \frac{22400 \cdot \frac{T_1}{273} \left[\frac{\dot{V}_{F,1} \cdot \rho_{F,1}}{60 \cdot W_{F,1}} + \frac{\dot{V}_{N_2,1} \cdot \rho_{N_2,1}}{60 \cdot W_{N_2,1}} \right]}{A_{nozzle}}. \quad (3.2)$$

Equation 3.2: In this equation, v_1 is the fuel stream velocity in cm/s , $\dot{V}_{F,1}$ is the volumetric fuel flow rate in ml/min and $\dot{V}_{N_2,1}$ is the volumetric nitrogen flow rate in Lpm , ρ is the density of the liquid or gas in g/ml , W is the molecular weight g/mol , T_1 is the fuel duct side temperature in Kelvin and CS is the cross section of the nozzle in cm^2 . The cross section of the nozzle is $A_{nozzle} = 0.3 \text{ cm}^2$.

For all procedures a constant co-flow air velocity of 47.6 cm/s was used. For the flame height experiments the fuel stream velocity was varied by changing the fuel flow rate and adjusting the nitrogen flow rate to keep the fuel mass fraction constant at 0.250.

$$Y_{F,1} = \frac{\dot{V}_{F,1} \cdot \rho_{F,1}}{\dot{V}_{F,1} \cdot \rho_{F,1} + \dot{V}_{N_2,1} \cdot \rho_{N_2,1}}. \quad (3.3)$$

In the equation 3.3 shows the calculation of the fuel mass fraction. The fuel mass fraction $Y_{F,1}$ is given by the the fuel flow rate $\dot{V}_{F,1}$, the fuel density $\rho_{F,1}$, the nitrogen flow rate $\dot{V}_{N_2,1}$, and the nitrogen density $\rho_{N_2,1}$.

The flame height experiments started at a fuel flow rate of 0.150 ml/min and the nitrogen flow rate was adjusted to keep the mass fraction of fuel in the mixture held at 0.25. For the first few steps, the fuel increment was set to 0.05 ml/min and when the flame was close to lift-off the increment was reduced to 0.01 ml/min . Once lift-off was achieved, the flow rate decreased to 0.150 ml/min and the experiment was repeated.

For the lift off hysteresis experiment the co-flow air velocity was also set to 47.6 cm/s . To demonstrate that lift off depended on the fuel mass fraction during the whole experiment, fuel stream velocity was held constant at 75 cm/s . The fuel flow was varied with each increment in nitrogen mass fraction such that this specific fuel stream velocity was held constant. To get the right fuel flow rate the Equation 3.2 was rearranged so that a constant nozzle velocity and a specific nitrogen flow rate one calculates the proper fuel flow rate as

$$\dot{V}_{F,1} = \frac{60 \cdot W_{F,1} \left[\frac{A_{nozzle} \cdot v_1}{22400 \cdot \frac{T_1}{273}} - \frac{\dot{V}_{N_2,1} \cdot \rho_{N_2,1}}{60 \cdot W_{N_2,1}} \right]}{\rho_{F,1}}. \quad (3.4)$$

3.2. Statistics

To get the mean value of the flame height and the confidence limits the following Equations 3.5, 3.6, 3.7 and 3.8 were used in this thesis. The probability value for the statistic calculations was chosen as 68.26 %.

Random errors can cause repeated measurements of one and the same measured variable

with the same measurement device, independent of one another with different distributed measured values x_i ($i = 1, 2, \dots, N < \infty$).

As estimate for the true value of the flame height x_w count the arithmetic mean value.

$$\bar{x} = \frac{1}{N} \sum_{i=1}^N x_i \quad (3.5)$$

To quantify the statistical spread of the measured value x_i the standard deviation s of \bar{x} is used.

$$s \cong \sqrt{\frac{\sum_{i=1}^N (x_i - \bar{x})^2}{N - 1}} \quad (3.6)$$

We get the standard deviation of the arithmetic mean value \bar{x} and the true value x_w from the equation 3.7 with

$$\bar{s} = \frac{t(P, N) s}{\sqrt{N}} \quad (3.7)$$

$t(P, N)$ as 'Confidence Factor' of the Student distribution by Gosset. Table 3.1 shows the 'Confidence Factor' $t(P, N)$ as function of the number of N of measurements and of the chosen probability P . Now we can specify an interval $\pm \bar{s}$ around the mean value \bar{x} called the 'Confidence Limit'. Inside this interval you can expect the true value x_w with the probability P .

$$x_w = \bar{x} \pm t(P, N) \sqrt{\frac{\sum_{i=1}^N (x_i - \bar{x})^2}{N - 1}} \quad (3.8)$$

$(\bar{x} + \bar{s})$ is the upper confidence limit and $(\bar{x} - \bar{s})$ is the lower confidence limit. [14]

Table 3.1.: t Distribution by William Sealy Gosset

t Distribution			
N	P = 68.26 %	P = 95 %	P = 99 %
2	1.84	12.71	63.7
3	1.32	4.30	9.9
4	1.20	3.18	5.8
5	1.15	2.78	4.6

Chapter 4.

Experiments

The experiments were conducted at atmospheric pressure and at 295 K ambient air temperature. During the whole experiment the vaporizer temperature ($T_{vapor} = 493\text{ K}$), fuel line temperature ($T_1 = 480\text{ K}$), air temperature ($T_2 = 480\text{ K}$), air flow rate ($\dot{V}_{air,2} = 140\text{ Lpm}$), ultra sonic nozzle temperature ($T_{us\ nozzle} = 328\text{ K}$), and the power output of the ultrasonic broadband generator were kept constant at ($P_{generator} = 0.5\text{ W}$).

For the flame height experiment also the mass fraction of fuel was kept constant at 0.25 and for the lift off hysteresis experiment the fuel stream velocity was constant at 75 cm/s .

By changing the fuel flow rate and the nitrogen flow rate one adjusts the nozzle velocity for the flame height experiment and the fuel mass fraction for the lift off hysteresis experiment.

4.1. Flame Height Experiments

The flame height experiment was carried out to study the dependency of flame height and fuel stream velocity. During this experiment the fuel mass fraction was kept constant at $Y_{F,1} = 0.25$. To obtain a constant fuel mass fraction it was necessary to change the fuel mass flow and the nitrogen mass flow in proper proportions by using Equation 3.3 and Equation 3.2. The changes were done by hand on the MKS mass flow controller unit and on the syringe pump control unit. To pay attention to the delay in the experimental system there was a waiting time of two minutes to ensure that the flame reached a steady condition before a picture was taken and data of the parameters were recorded.

The experiment started at a low fuel stream velocity and by increasing the fuel mass flow and the nitrogen mass flow the flame lifted off at a certain velocity. After the lift off

the fuel stream velocity was lowered to the starting point. Every point of the first session was repeated again to get an overall number of five runs for each fuel and each surrogate.

4.2. Lift-Off Hysteresis Experiments

During the flame height experiment it was obvious that there is a hysteresis between lift off and return of the flame depending on the fuel stream velocity. A previous study [17] showed the hysteresis for a methane flame by increasing the fuel stream velocity. It was the idea to see if this lift off phenomena is only depending on the fuel stream velocity or also on the fuel mass fraction. The lift off hysteresis experiment was carried out at a constant fuel stream velocity $v_1 = 75 \text{ cm/s}$ and constant oxidizer velocity $v_2 = 47.6 \text{ cm/s}$. To keep the fuel stream velocity constant we used Equation 3.4 by changing the nitrogen mass flow slightly and adjusting the fuel mass flow to the exact value from the equation.

After ignition the flame was found close to the nozzle tip. The next step was to increase the nitrogen mass flow and decrease the fuel mass flow to get a mixture with lower Y_F , 1, i.e. decreasing the fuel mass fraction, at a constant fuel stream velocity. There was a delay of two minutes between changing the mass flows and taking the pictures due to the inertia of the whole system. So after changing the flows the timer was set to two minutes and when the alarm went off a picture of the flame was taken and all parameters were recorded into a MS Excel spreadsheet.

As the flame lifted off the fuel mass fraction was increased again until the flame returned to the nozzle tip. To get representative data the whole lift off experiment for each of the three fuels and five surrogates was repeated five times.

Not only the lift off height was important during the hysteresis experiment. There was also a look for the development of the flame height during lift-off. So for every step there are two important quantities to record the lift off height on the one hand and the flame height on the other.

4.3. Diffusion Flame Problem by Burke-Schumann

“Burke and Schumann gave the first successful detailed analysis of a diffusion-flame problem in 1928” [20]. The Burke-Schumann problem is illustrated in Figure 4.1 where fuel comes from a cylindrical tube into concentric cylindrical duct through which oxidizer is flowing. A flame, established at the tip of the tube and either extends to the wall of the outer duct, is called the underventilated case and the case where the flame converges to the axis is called overventilated. The flame height is defined as the axial distance from the tip of the tube to the point at which the flame reaches either the wall of the outer duct or the axis. The flame height is required for the design of burners of this type. Burke and Schumann obtained fairly accurate predictions of the flame height and the flame shape of the flame in laminar flow [20].

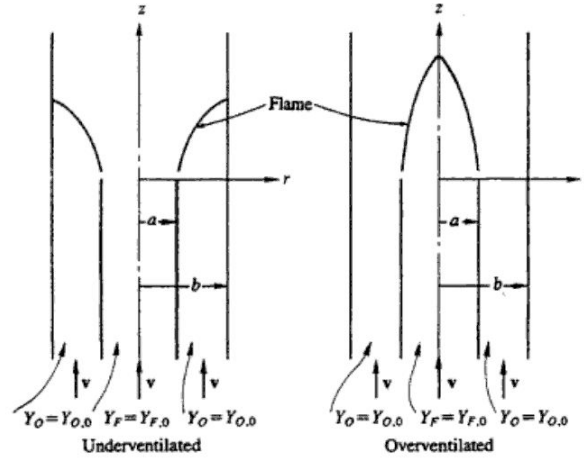


Figure 4.1.: A diffusion flame at the mouth of a tube in a duct for the underventilated and the overventilated case. Y_O is the mixture strength of oxidizer and Y_F is the mixture strength of fuel [20].

Equation 4.1 shows the whole expression for the flame shape for the underventilated and for the overventilated case seen in Figure 4.2.

$$\gamma = (1 + \nu) c^2 - \nu + 2(1 + \nu) c \sum_{n=1}^{\infty} \frac{1}{\varphi_n} \frac{J_1(c\varphi_n)}{[J_0(\varphi_n)]^2} J_1(\varphi_n \xi) e^{-\varphi_n^2 \eta} \quad (4.1)$$

Setting $\gamma = 0$ in the Equation 4.1 provides a relation between ξ and η that defines the locus of the flame. The shape of the surface in this manner is shown in Figure 4.2 for $c = \frac{1}{2}$ and different values of ν .

To solve Equation 2.1 we have to know the following dimensionless coordinates and reduced parameters

$$\eta \equiv \frac{zD}{vb^2} \quad (4.2)$$

and

$$\xi \equiv \frac{r}{b} \quad (4.3)$$

and the reduced parameters

$$c \equiv \frac{a}{b} \quad (4.4)$$

and

$$\nu \equiv \frac{Y_{O_2,2}W_{F,1}\nu_{F,1}}{Y_{F,1}W_{O_2,2}\nu_{O_2,2}} \quad (4.5)$$

the reduced variable

$$\gamma \equiv \frac{\beta W_{F,1}\nu_{F,1}}{Y_{F,1}} \quad (4.6)$$

and the boundary condition for β

$$\beta = \frac{Y_{F,1}}{W_{F,1}\nu_{F,1}} \quad \text{at } z = 0, \quad 0 \leq r < a. \quad (4.7)$$

By rearranging Equation 4.2 we get the equation for the absolute flame height z ,

$$z = \eta \frac{vb^2}{D} \quad (4.8)$$

The flame height calculated with Equation 4.8 can be found in the Figure 4.2 on the far left side at $\xi = 0$.

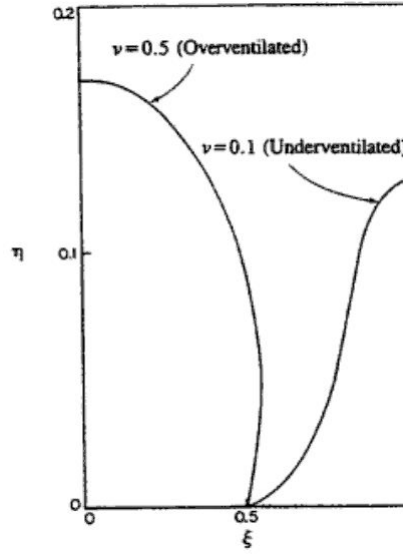


Figure 4.2.: Flame shapes for the Burke-Schumann problem with $c = \frac{1}{2}$ [20].

Figure 4.2 shows the flame shape for an overventilated and an underventilated flame. On the x-axis we can see the dimensionless flame height η and on the y-axis the dimensionless distance ξ from the vertical flame center line. c is the ratio between nozzle and outer duct radius. In this figure c is 0.5 and ν is the mass ratio of fuel and oxidizer. Low numbers of ν indicate a fuel rich mixture and high numbers a fuel lean mixture [20].

Because of the fact, that in our case c is small it was necessary to calculate several terms of the Bessel functions $J_0(\phi_n)$ and $J_1(c\phi_n)$ to get z . After calculating twenty five zeros of $J_1(\phi)$ we got ϕ_1 through ϕ_{25} . With the rearranged Equation 4.1 and setting $\gamma = 1$ and $\xi = 0$ for the overventilated case we get

$$\frac{\nu - 2(1 + \nu)c}{(1 + \nu)c^2} = \sum_{n=1}^{25} \frac{1}{\phi_n} \frac{J_1(c\phi_n)}{[J_0(\phi_n)]^2} e^{-\phi_n^2 \eta}. \quad (4.9)$$

Now the only unknown in Equation 4.9 is η and by solving this equation we got the value of η . To calculate the flame hight it was also necessary to define a diffusion coefficient for each fuel and surrogate. To do this the approach

$$\frac{D_{AB}}{D_{CD}} = \frac{\sqrt{\frac{1}{W_A} + \frac{1}{W_B}}}{\sqrt{\frac{1}{W_C} + \frac{1}{W_D}}} \quad (4.10)$$

from [2] was used. In Equation 4.10 D_{AB} is the diffusion coefficient of fuel A and the oxidizer B , D_{CD} is the diffusion coefficient of fuel C and the oxidizer D , W_A and W_C are the molecular weights of the fuels, and W_B and W_D are the molecular weights of the oxidizers. As reference the diffusion coefficient of n-heptane ($D_{AB} = 2.000$) was used.

Table 4.1.: φ_n , $J_0(\varphi_n)$, $J_1(c\varphi_n)$ and graph points for η of JP-8.

n	φ_n	$J_0(\varphi_n)$	$J_1(c\varphi_n)$	graph point
1	3.83	-0.403	0.111	0.169
2	7.02	0.300	0.200	0.265
3	10.17	-0.250	0.284	0.308
4	13.32	0.218	0.360	0.298
5	16.47	-0.196	0.427	0.252
6	19.62	0.180	0.483	0.189
7	22.76	-0.167	0.528	0.127
8	25.90	0.157	0.559	0.078
9	29.05	-0.148	0.577	0.043
10	32.20	0.141	0.582	0.021
11	35.32	-0.134	0.572	0.010
12	38.49	0.129	0.549	0.004
13	41.60	-0.124	0.514	0.002
14	44.78	0.119	0.468	0.001
15	47.91	-0.115	0.412	0.000

Table 4.1 shows the first fifteen φ , $J_0(\varphi)$, $J_1(c\varphi)$, and graph points seen in Figure 4.3 for JP-8 and $\eta = 3.617 \cdot 10^{-3}$.

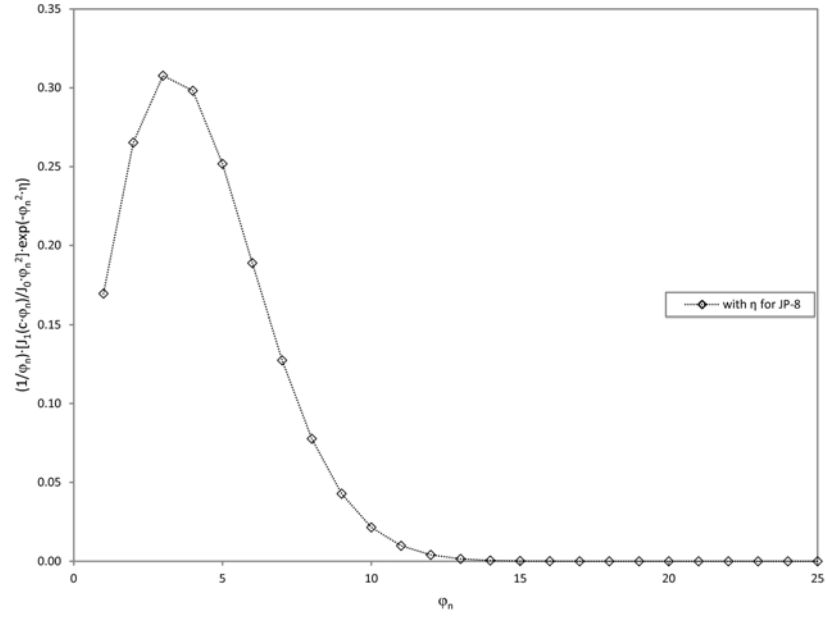


Figure 4.3.: Sumfunction of Equation 4.6 with increasing ϕ_n

Figure 4.3 illustrates the need of several terms of the sum function in Equation 4.6. Here we can see that after ϕ_{14} the sum function reaches zero level. The x-axis shows the number n of φ and the y-axis the value of the expression in sum function for each φ_n .

Chapter 5.

Experimental Results

In the following chapter we summarize the flame height and lift off experimental results as well as for the diffusion flame problem by Burke-Schumann. The detailed experimental data and pictures of the flames can be found in Appendix A and Appendix B.

5.1. Flame Height Experiment

The first experiment for this thesis was the measurement of the flame height for different fuels and surrogates at constant co-flow air velocity v_2 and fuel mass fraction $Y_{F,1}$. Measurement was started at a fuel flow rate of $\dot{V}_{F,1} = 0.150 \text{ ml/min}$ with the proper flow rate of nitrogen for each fuel tested. This resulted in initial flame heights between 8 mm and 10 mm as seen in Figure 5.1 and Figure 5.2. With increasing fuel flow rate also the nitrogen flow rate increases and therefore the fuel stream velocity increases as well to keep the fuel mass fraction $Y_{F,1}$ constant. Higher fuel stream velocities resulted in increased flame heights. The last measurement of the flame height was done one condition before we reached the lift-off fuel stream velocity.

The temperature of the oxidizer duct and the fuel duct temperature were kept always constant at $T_1 = T_2 = 480 \text{ K}$ so that there is no temperature difference between air stream and fuel/nitrogen stream during the event of mixture in the co-flow burner. As mentioned before, between increasing the fuel stream velocity and acquiring new data for the new conditions there was a delay of two minutes for flame stabilization due to the inertia of the system, for example the long vaporizer and fuel line.

5.1.1. Flame Height Results of Fuels

Figure 5.1 shows the flame height as a function of the fuel stream velocity v_1 for JP-8, Fischer-Tropsch IPK Sasol and Fischer-Tropsch Shell GTL. The definition for the flame height measurement can be found in Section 2.2. At the lowest nozzle velocity all three fuels showed a similar flame height of $9 \text{ mm} \pm 1 \text{ mm}$. After increasing the nozzle velocity JP-8 tends to have a bigger flame height than FT IPK Sasol and FT Shell GTL. The nozzle velocity for lift-off for JP-8 and FT IPK Sasol is similar and the flame height before lift-off differ about 5 mm . However, FT Shell GTL has a very high flame and a very high lift-off fuel stream velocity compared to JP-8 and FT IPK Sasol.

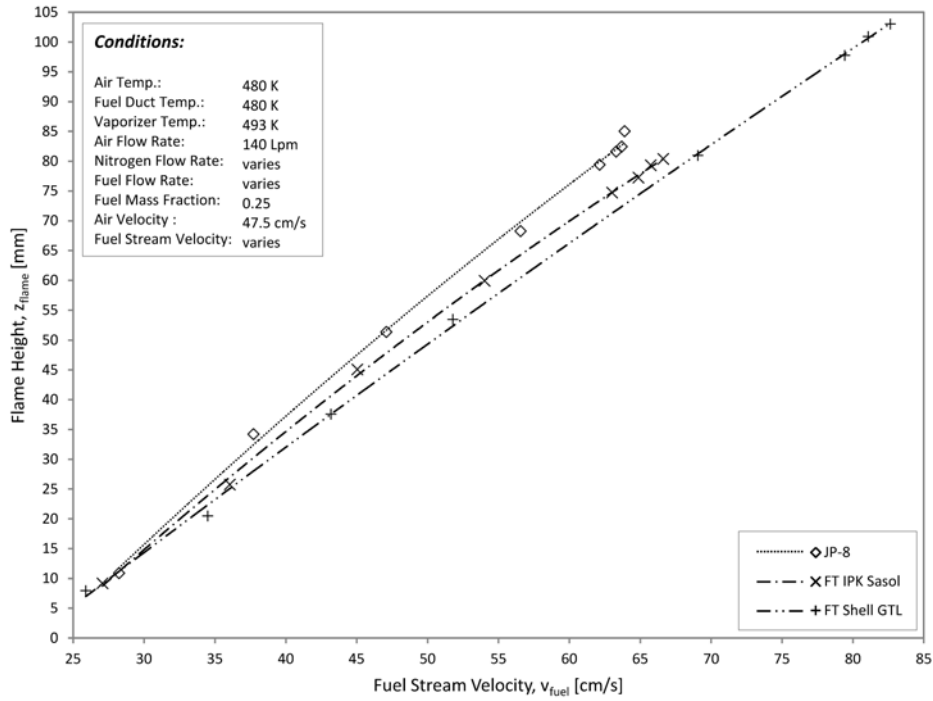


Figure 5.1.: Comparison of the flame height at constant fuel mass fraction $Y_{F,1} = 0.25$ as a function of the fuel stream velocity. The figure shows data for JP-8, FT IPK Sasol, and FT Shell GTL. The symbols represent experimental data and the lines are of polynomial second order best fit curves.

FT IPK Sasol is derived from coal and FT Shell GTL from natural gas [8]. The content of iso-paraffins and cyclo-paraffins is higher in FT IPK Sasol and the amount of normal paraffins is bigger in FT Shell GTL. Both of them have not a significant aromatic content. However, JP-8 has a lot of different hydrocarbons, an aromatic content of approximately 18.8 vol%, and many other substances, for example metal, due to the refining process of crude oil. This explains why JP-8 has one of the brightest flame during the experiment and also the most content of soot as you can see in Figure B.4.

5.1.2. Flame Heights of Surrogates

The second part of the flame height experiment was the study of the behavior of surrogates at different fuel stream velocities. Figure 5.2 shows the flame height as a function of fuel stream velocity for Aachen surrogate, JP-8 Surrogate C, SERDP surrogate, Modified SERDP Surrogate, and Gasoline Surrogate C. This figure also shows the JP-8 curve as reference.

From this figure we see that the surrogates differ in flame height by ± 5 mm over a very long period of fuel stream velocity. Only close to lift-off the Modified SERDP Surrogate has the highest flame of all surrogates and also the lift-off fuel stream velocity is slightly higher than the velocity of the other four surrogates. It also can be seen that Aachen Surrogate, SERDP Surrogate, and JP-8 Surrogate are very similar in terms of flame height and lift-off fuel stream velocity.

As we can see from this figure JP-8 has the highest flame height of all tested fuels and also the lowest lift-off fuel stream velocity.

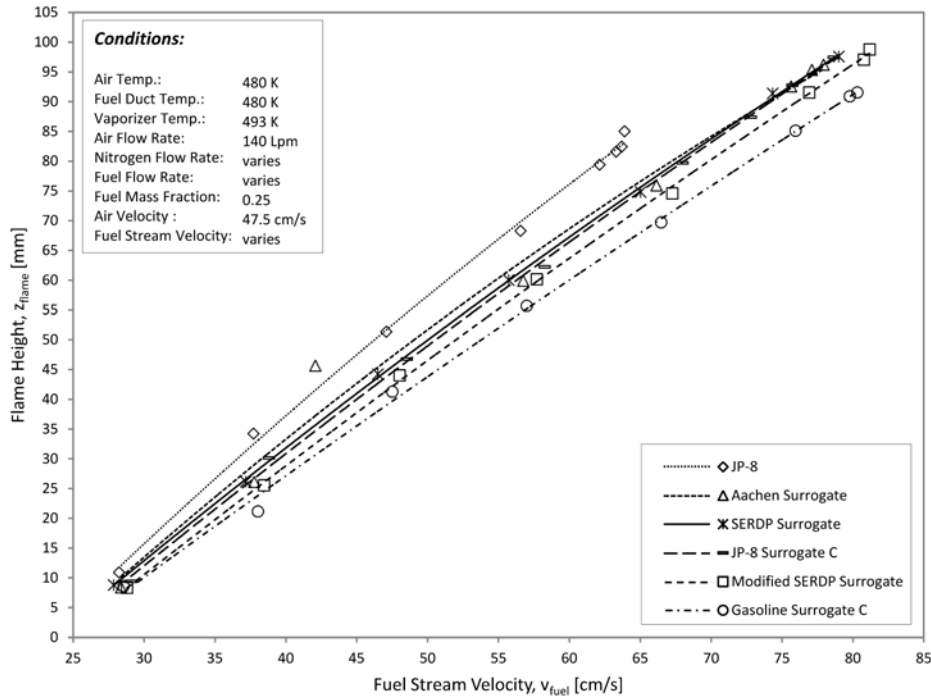


Figure 5.2.: Comparison of the flame height at constant fuel mass fraction $Y_{F,1} = 0.25$ as a function of the fuel stream velocity. The figure shows data for JP-8, Aachen Surrogate, SERDP Surrogate, JP-8 Surrogate C, Modified SERDP Surrogate, and Gasoline Surrogate C. The symbols represent experimental data and the lines are of polynomial second order best fit curves.

The results for the surrogates are obvious because Aachen Surrogate, JP-8 Surrogate

C, and SERDP Surrogate have a higher content of aromatics than Gasoline Surrogate C. Gasoline Surrogate C is a four component compound containing n-paraffin, iso-paraffin, cyclo-paraffin, and one aromatic compound. The aromatic content in Gasoline Surrogate C with 13 mol% is lower than the contents of Aachen Surrogate, 26.2 mol%, JP-8 Surrogate C, 28.3 mol%, and SERDP Surrogate, 23 mol%.

5.1.3. Conclusion of the Flame Height Experiment

We found a good match between FT IPK Sasol, Aachen Surrogate, JP-8 Surrogate C, SERDP Surrogate, and FT Shell GTL as seen in Figure 5.3. FT Shell GTL, Aachen Surrogate, JP-8 Surrogate C, and SERDP Surrogate have a similar flame height over a wide interval of fuel stream velocity from 29 cm/s through 78 cm/s . FT IPK Sasol and Aachen Surrogate, JP-8 Surrogate C, and SERDP Surrogate have a smaller interval from 29 cm/s through 66 cm/s with a good match.

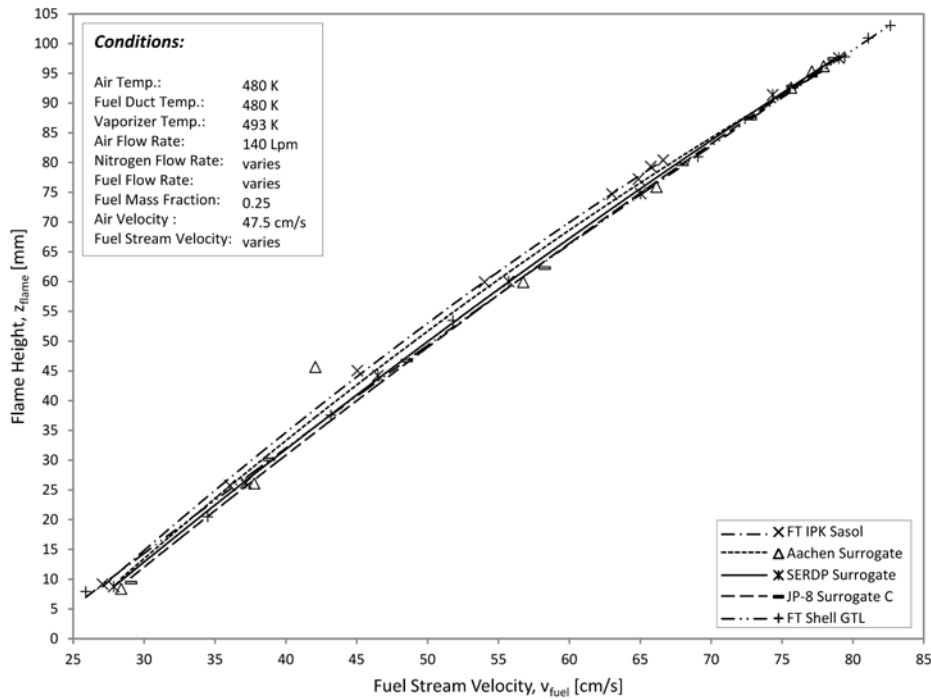


Figure 5.3.: Comparison of the flame height at constant fuel mass fraction $Y_{F,1} = 0.25$ as a function of the fuel stream velocity. The figure shows the data for FT IPK Sasol, Aachen Surrogate, SERDP Surrogate, JP-8 Surrogate C, and FT Shell GTL. The symbols represent experimental data and the lines are of polynomial second order best fit curves.

Furthermore, its surprising that JP-8 and FT IPK Sasol have their lift-off point around 65 cm/s at a similar flame height ± 5 mm and the flame height of FT Shell GTL reaches

up to 103 *mm* at a fuel stream velocity of 83 *cm/s*. The fraction of iso-paraffines of FT IPK Sasol is 88 mass% and it is significant higher than for FT Shell GTL with a content of 57 mass% [8]. Furthermore has FT IPK Sasol a higher fraction of cyclo-paraffines and a lower fraction of normal-paraffines as FT Shell GTL.

5.2. Lift-Off Hysteresis Experiment

The second part of this thesis was developed during the flame height experiment because of the fact that there was a hysteresis between lift-off and return of the flame to the nozzle tip. The lift-off during the flame height experiment was depending on the fuel stream velocity so we posed the question if the lift off could also depend on the fuel mass fraction as well. This was the initial question for the second experiment, the lift-off hysteresis experiment. During the experiment we measured the lift-off heights and it was also possible to measure the flame heights during lift-off.

The experiments were carried out with a fuel stream velocity of $v_1 = 75 \text{ cm/s}$, a co-flow air velocity of $v_2 = 47.6 \text{ cm/s}$ and a fuel and air temperature of $T_1 = T_2 = 480 \text{ K}$. The starting point was a flame with a fuel mass fraction close to lift-off conditions and the end of the experiment was reached when the flame returned to the nozzle tip by increasing the fuel mass fraction again. Nevertheless, the first step was to decrease the fuel mass fraction $Y_{F,1}$ to reach the flame lift-off condition, in this experiment the lift-off fuel mass fraction. After lift-off the fuel mass fraction was increased in several steps and the lift-off heights and flame heights were recorded. This experiment was done five times for each fuel and surrogate to get a proper amount of sample for the statistic analysis.

5.2.1. Lift-Off Hysteresis of Fuels

Figure 5.4 shows the lift-off height during the experiment for FT IPK Sasol, JP-8 and FT Shell GTL as a function of the fuel mass fraction. The dotted lines with the arrows show the direction of the lift-off height development for JP-8 and how the flame lift-off height behaves when it comes from a high fuel mass fraction to a low fuel mass fraction.

We are reaching the lift-off conditions from the right side by decreasing the fuel mass fraction $Y_{F,1}$. All three fuels have their lift-off heights around $184 \text{ mm} \pm 2.5 \text{ mm}$. Nevertheless the fuel mass fraction at which lift-off occurs reach from 0.359 for FT Shell GTL over 0.378 for JP-8 to 0.394 for FT IPK Sasol.

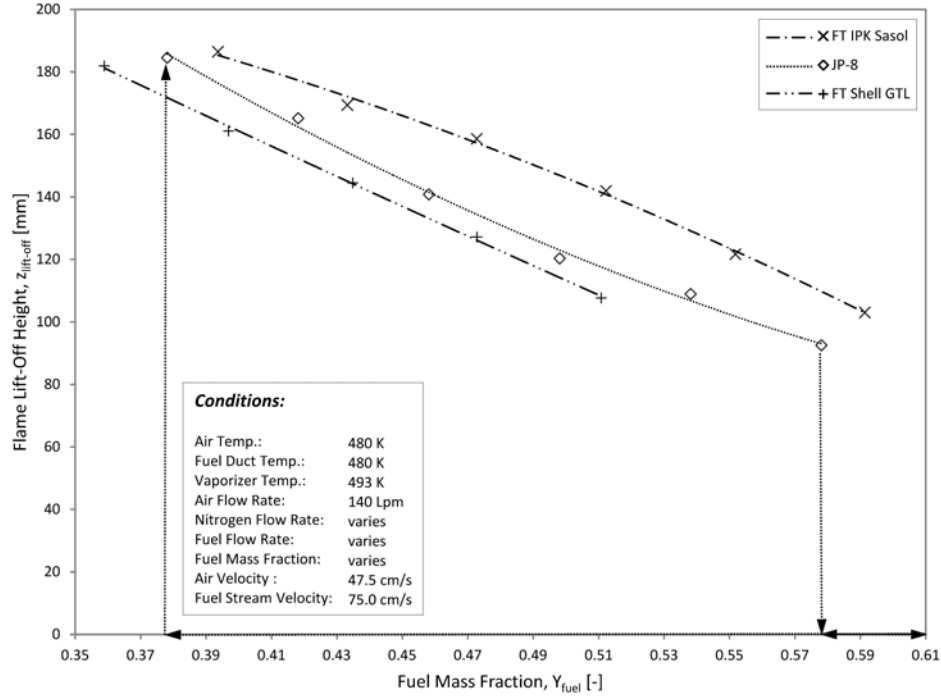


Figure 5.4.: Comparison of the lift-off height at constant fuel stream velocity $v_1 = 75 \text{ cm/s}$ as a function of the fuel mass fraction. The figure shows data for FT IPK Sasol, JP-8 and FT Shell. The symbols represent experimental data and the lines are of polynomial second order best fit curves.

Slightly different are the conditions for the flame return conditions. The flame for FT Shell GTL returned to the nozzle tip at a fuel mass fraction of 0.511. In comparison the flame for JP-8 and FT IPK Sasol returned at 0.578 and 0.591 respectively. The lift-off height before flame return was for FT Shell GTL higher than as for the other two kerosene fuels.

5.2.2. Lift-Off Hysteresis of Surrogates

In the Figure 5.5 the behavior of Aachen Surrogate, JP-8 Surrogate C, SERDP Surrogate, Modified SERDP Surrogate, and Gasoline Surrogate C flame lift-off height is shown as a function of fuel mass fraction. The JP-8 curve shown in the figure is for reference purposes.

We found a good match for lift-off heights between Aachen Surrogate and JP-8. The lift-off conditions are very similar and the lift-off height differs only by 2.3 mm only JP-8 returns to the nozzle tip at a lower fuel mass fraction. The fuel mass fraction for flame return for JP-8 is 0.550 and the fuel mass fraction for Aachen Surrogate is 0.578.

Modified SERDP Surrogate has the lowest lift-off height of the three surrogates and Surrogate C the highest one. Also lift-off occurs for the Modified SERDP Surrogate at a lower fuel mass fraction. Gasoline Surrogate C and Aachen Surrogate have with 0.371 and 0.372 nearly the same fuel mass fraction at the lift-off point.

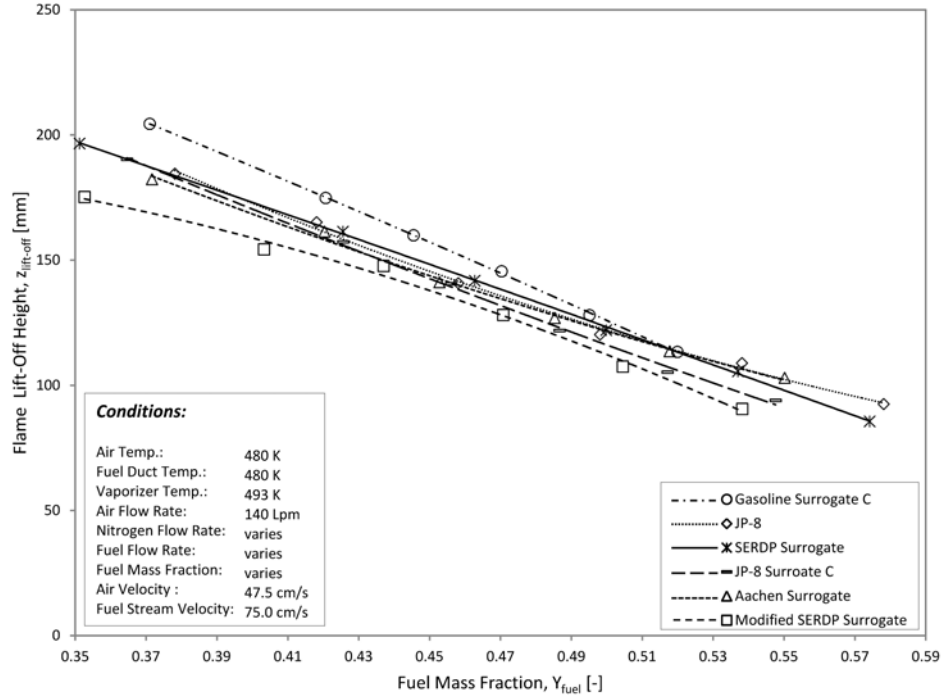


Figure 5.5.: Comparison of the lift-off height at constant fuel stream velocity $v_1 = 75 \text{ cm/s}$ as a function of the fuel mass fraction. The figure shows data for Gasoline Surrogate C, JP-8, SERDP Surrogate, JP-8 Surrogate C, Aachen Surrogate, and Modified SERDP Surrogate. The symbols represent experimental data and the lines are of polynomial second order best fit curves.

5.2.3. Conclusion for Lift-Off Hysteresis Experiment

This kind of experiments were done the first time for kerosene fuels and surrogates. So it was quite interesting to see the results and to see if there are any agreements between the fuels and surrogates. We found out that JP-8 and Aachen Surrogate, JP-8 Surrogate C, and SERDP Surrogate match best in terms of lift-off fuel mass fraction and lift-off height. For the other fuels we were not able to find some good matches.

5.3. Flame Height during Lift-Off Experiments

Beside the lift-off height measurements it was also obvious and interesting to measure the flame height during lift-off. The flame height measurements were done for all three fuels and all five surrogates. For the conditions during this experiment please see Section 5.2.

5.3.1. Flame Height of Fuels during Lift-Off

Figure 5.6 shows the curves for the flame height for JP-8, FT Shell GTL and FT IPK Sasol as a function of the fuel mass fraction displayed.

The dotted line with the arrows shows the development of the flame at the nozzle until the fuel mass fraction reaches the lift-off condition. The height of the flame at the nozzle decreases with decreasing fuel mass fraction and after lift-off the flame height decreases about a factor three of the last flame height before lift-off. With increasing fuel mass fraction and decreasing lift-off height the flame height increases.

There is no significant match between the three kerosene fuels. They differ in terms of lift-off fuel mass ratio and flame height during the whole experiment.

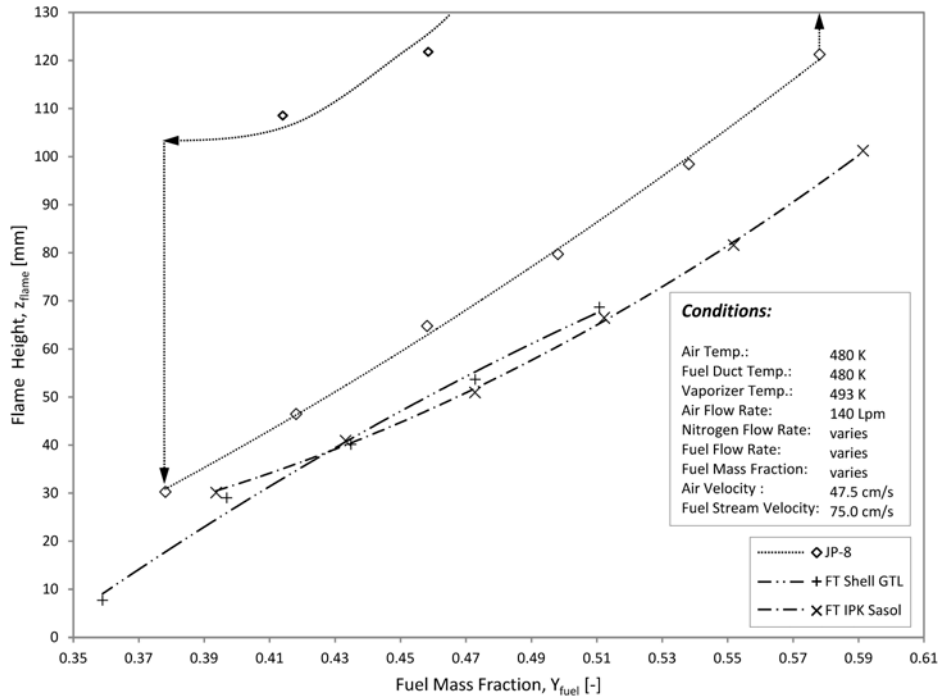


Figure 5.6.: Comparison of the flame height during lift-off height at constant fuel stream velocity $v_1 = 75 \text{ cm/s}$ as a function of the fuel mass fraction. The figure shows data for JP-8, FT Shell and FT IPK Sasol. The symbols represent experimental data and the lines are of polynomial second order best fit curves.

5.3.2. Flame Height of Surrogates during Lift-Off

Figure 5.7 shows the flame height for a Modified SERDP surrogate, JP-8 Surrogate C, SERDP Surrogate, Aachen surrogate and a Gasoline Surrogate C flame as a function of fuel mass fraction. This figure also shows the JP-8 curve as reference.

JP-8, Aachen Surrogate, JP-8 Surrogate C, and Gasoline Surrogate C tend to have a similar lift-off fuel mass fraction as discussed before in Section 5.2. All five surrogates have different flame heights and different fuel mass fraction when it comes to flame return conditions only the trend of the increasing flame height for JP-8, Aachen Surrogate, and Gasoline Surrogate C looks similar. Only JP-8 Surrogate C and Modified SERDP Surrogate has a similar flame height between 0.43 and 0.53 fuel mass fraction $Y_{F,1}$.

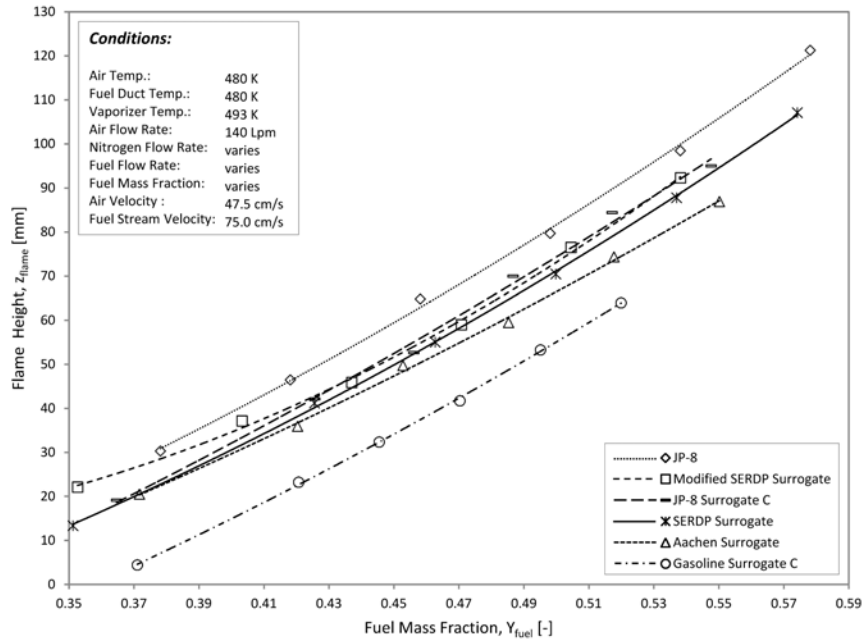


Figure 5.7.: Comparison of the flame height during lift-off height at constant fuel stream velocity $v_1 = 75 \text{ cm/s}$ as a function of the fuel mass fraction. The figure shows data for JP-8, Modified SERDP Surrogate, JP-8 Surrogate C, SERDP Surrogate, Aachen Surrogate, and Gasoline Surrogate C. The symbols represent experimental data and the lines are of polynomial second order best fit curves.

5.3.3. Conclusion of Flame Height during Lift-Off Experiment

It was difficult to find matches between the kerosene fuels and surrogates for the flame height during lift-off. The trend of the flame height development with increasing fuel mass fraction between JP-8, Aachen Surrogate, and Gasoline Surrogate C is a more or less good match for this experiment.

5.4. Diffusion Flame Problem by Burke-Schumann

The data presented in Section 4.3 were used in this part of the thesis. The main idea was to show that the trend between experiments and calculates are identical. Calculations were done for all fuels and all surrogates as well as for the pure components of the surrogates.

Table 5.1 present the approximated H/C formula, the molecular weight, η , ν , and the diffusion coefficient for each fuel for a fuel mass fraction $Y_{F,1}$ of 0.25.

Table 5.1.: Burke-Schumann Problem for Fuels and Surrogates Calculation Data - η , ν , and diffusion coefficient at a fuel mass fraction $Y_{F,1} = 0.25$.

Fuel	Approximated Formula	Molecular Weight [g/mol]	η [-]	ν [-]	Diffusion Coeff. [cm^2/s]
JP-8	$C_{11}H_{21}$	147.83	$3.617 \cdot 10^{-3}$	0.2650	1.920
FT Shell GTL	$C_{10.04}H_{22.05}$	142.77	$3.587 \cdot 10^{-3}$	0.2674	1.926
FT IPK Sasol	$C_{11.41}H_{24.26}$	161.84	$3.577 \cdot 10^{-3}$	0.2684	1.906
Aachen Surrogate	$C_{9.77}H_{19.72}$	137.24	$3.534 \cdot 10^{-3}$	0.2719	1.934
JP-8 Surrogate C	$C_{9.48}H_{18.14}$	132.14	$3.503 \cdot 10^{-3}$	0.2747	1.941
SERDP Surrogate	$C_{10.56}H_{20.22}$	155.58	$3.505 \cdot 10^{-3}$	0.2902	1.912
Modified SERDP Surrogate	$C_{10.42}H_{20.31}$	145.62	$3.515 \cdot 10^{-3}$	0.2737	1.923
Gasoline Surrogate C	$C_{7.34}H_{14.96}$	103.27	$3.541 \cdot 10^{-3}$	0.2714	1.993

Tabel 5.2 shows the same data as Table 5.1 but for the pure surrogate components for a fuel mass fraction $Y_{F,1}$ of 0.25.

Table 5.2.: Burke-Schumann Problem for Pure Hydrocarbons Calculation Data - η , ν , and diffusion coefficient at a fuel mass fraction $Y_{F,1} = 0.25$.

Hydrocarbon	Formula	Molecular Weight [g/mol]	η [-]	ν [-]	Diffusion Coeff. [cm^2/s]
n-Heptane	C_7H_{16}	100.20	$3.612 \cdot 10^{-3}$	0.2653	2.000
n-Decane	$C_{10}H_{22}$	142.28	$3.589 \cdot 10^{-3}$	0.2673	1.927
n-Dodecane	$C_{12}H_{26}$	170.33	$3.579 \cdot 10^{-3}$	0.2682	1.898
iso-Octane	C_8H_{18}	114.23	$3.604 \cdot 10^{-3}$	0.2662	1.970
Methylcyclohexane	C_7H_{14}	98.19	$3.531 \cdot 10^{-3}$	0.2724	2.005
Toluene	C_7H_8	92.14	$3.258 \cdot 10^{-3}$	0.2982	2.021
Trimethylbenzene	$C_{12}H_{12}$	120.19	$3.321 \cdot 10^{-3}$	0.2917	1.959
Xylene	C_8H_{10}	106.17	$3.258 \cdot 10^{-3}$	0.2945	1.986

To verify the calculation of the flame height for the pure hydrocarbons data from flame height experiments done by Tei Newman-Lehman are used. Mr. Lehman-Newman recorded flame heights for all the pure hydrocarbons. The flame heights are shown in the Table 5.3 below. All the experiments for this hydrocarbons were carried out at a fuel mass fraction $Y_{F,1}$ of 0.4.

Table 5.3.: Burke-Schumann Problem for Pure Hydrocarbons Calculation Data- η , ν , and diffusion coefficient at fuel mass fraction $Y_{F,1} = 0.4$ in comparison with experimental flame height data.

Hydrocarbon	Flame Height Experimental [mm]	Flame Height Calculated [mm]	Fuel Stream Velocity, v_1 [cm/s]	η [-]	ν [-]
n-Heptane	39.5	74.3	24.5	$5.543 \cdot 10^{-3}$	0.1658
n-Decane	35.8	72.9	23.3	$5.507 \cdot 10^{-3}$	0.1671
n-Dodecane	35.1	72.4	22.9	$5.485 \cdot 10^{-3}$	0.1676
iso-Octane	39.9	75.3	24.6	$5.531 \cdot 10^{-3}$	1.970
Methylcyclohexane	35.4	72.3	24.5	$5.409 \cdot 10^{-3}$	0.1702
Toluene	59.4	66.8	24.8	$4.975 \cdot 10^{-3}$	0.1865
Trimethylbenzene	55.8	84.2	29.7	$5.078 \cdot 10^{-3}$	0.1823
m-Xylene	53.5	82.1	29.6	$5.031 \cdot 10^{-3}$	0.1841
o-Xylene	55.3	84.0	30.3	$5.031 \cdot 10^{-3}$	0.1841

We can see in Table 5.3 that there is a difference between the measured height and the calculated flame height but we could prove the trend of the flame height development for each hydrocarbon. The flame height of toluene was difficult to measure because of the large soot region of the flame at this specific fuel mass fraction.

5.4.1. Flame Height for Diffusion Flame Problem by Burke-Schumann

Figure 5.8 shows the calculated flame height of JP-8, Aachen Surrogate, JP-8 Surrogate C, SERDP Surrogate, Modified SERDP Surrogate, and Gasoline Surrogate C as a function of the fuel stream velocity v_1 and it can be compared with Figure 5.2.

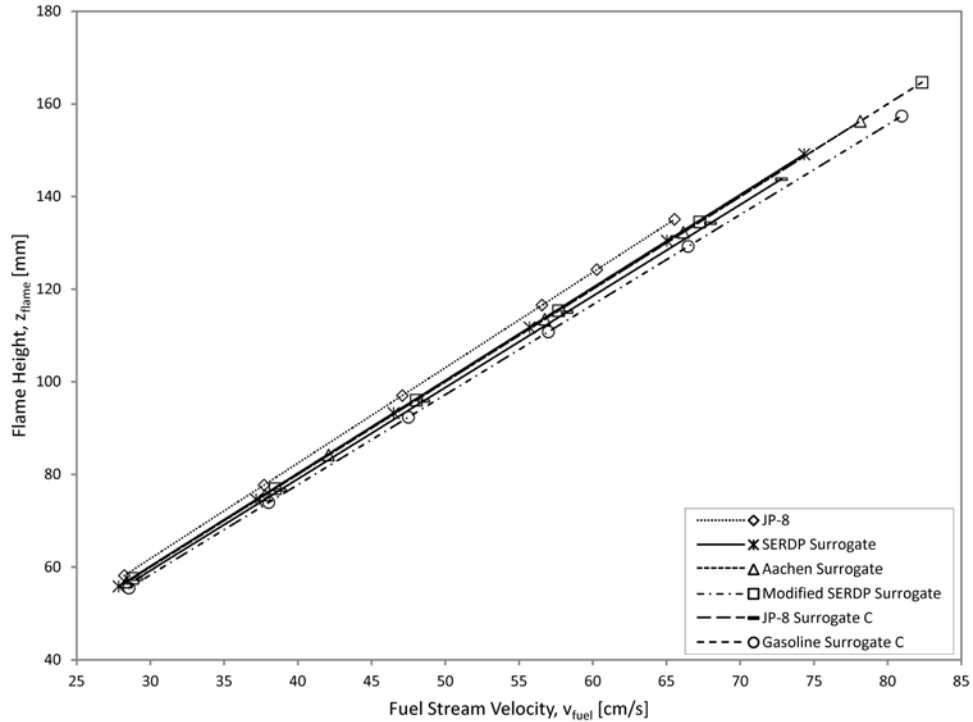


Figure 5.8.: Flame height for the diffusion flame problem by Burke-Schumann for JP-8, SERDP Surrogate, Aachen Surrogate, Modified SERDP Surrogate, JP-8 Surrogate C, and Gasoline Surrogate c as a function of the fuel stream velocity.

Figure 5.9 shows the calculated flame height for JP-8, FT Shell GTL, and FT IPK Sasol as a function of the fuel stream velocity v_1 and it can be compared with Figure 5.1.

In Figure 5.10 the calculated flame height for all pure components of the surrogates is shown as a function of the fuel stream velocity v_1 .

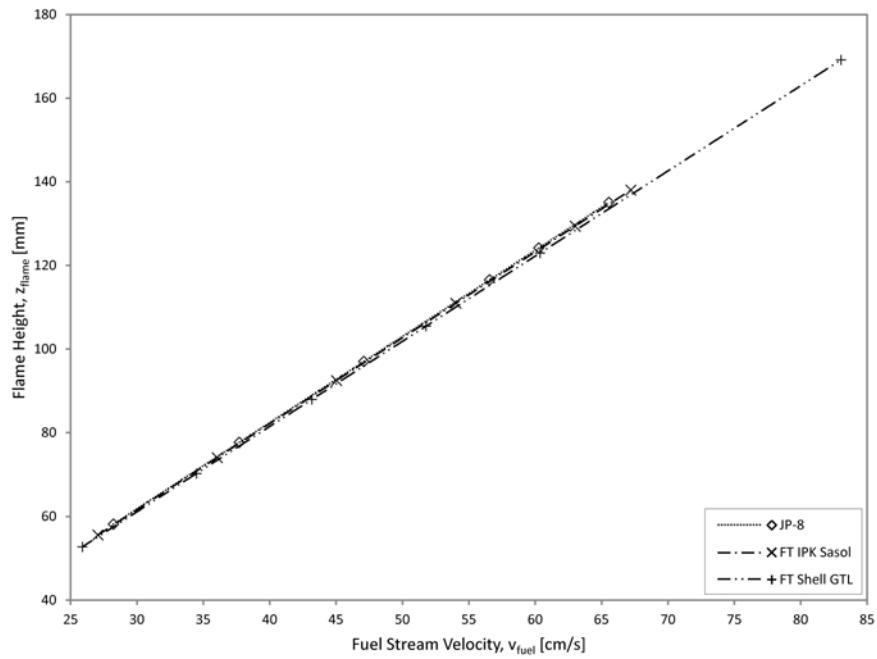


Figure 5.9.: Flame height for the diffusion flame problem by Burke-Schumann for JP-8, FT IPK Sasol, and FT Shell GTL as a function of the fuel stream velocity.

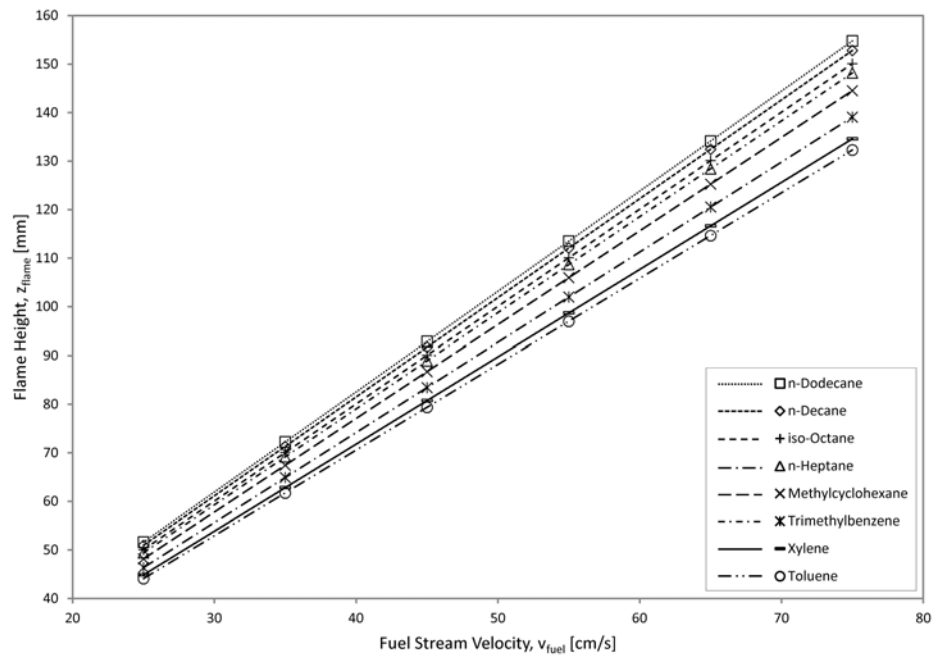


Figure 5.10.: Flame height for the diffusion flame problem by Burke-Schumann for pure n-Dodecane, n-Decane, iso-Octane, n-Heptane, Methylcyclohexane, Trimethylbenzene, and Toluene as a function of the fuel stream velocity.

5.4.2. Conclusion of Flame Height for Diffusion Flame Problem by Burke-Schumann

The absolute value of the flame height carried out with the Burke-Schumann equation is higher as the actual one measured during the flame height experiments. This is because the Burke-Schumann equation does not take the reactions close to the nozzle tip into account. The important thing during this thesis was to show that the trend of the flame height for both the experiment and the calculation is the same. As one can see in Figure 5.8 and Figure 5.9 the calculation results present the same trend as the flame heights during the experiments.

Figure 5.11 presents the comparison of flame heights calculated by Equation 5.1 for very small c [20], by the calculation from Section 4.3 and measured during the experiments for Aachen Surrogate, JP-8 Surrogate C, and SERDP Surrogate.

$$z = \frac{va^2}{D} \frac{(1 + \nu)}{4\nu} \quad (5.1)$$

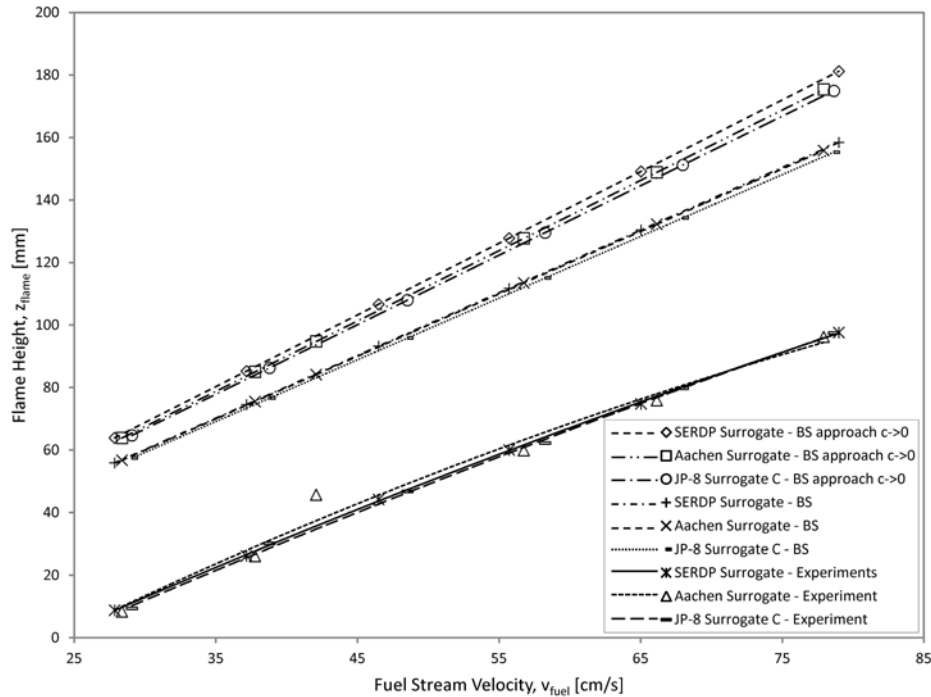


Figure 5.11.: Comparison flame height calculation for small c , flame height calculation with twenty five terms, and measured flame heights during the experiments as a function of fuel stream velocity v_1 of SERDP Surrogate, Aachen Surrogate, and JP-8 Surrogate C.

We could prove that in our case for $c = 0.0583$ the calculation with the twenty five terms presents the trend of the flame height development best.

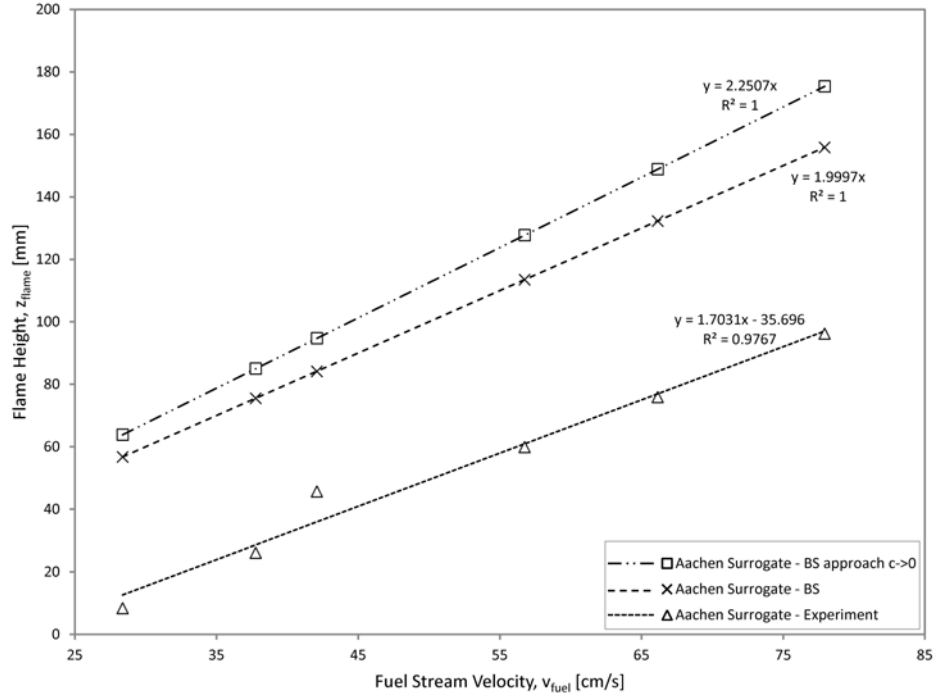


Figure 5.12.: Comparison flame height calculation for small c , flame height calculation with twenty five terms, and measured flame heights during the experiments as a function of fuel stream velocity v_1 of Aachen Surrogate. The lines are linear best fit curves with coefficient of determination shown and linear equation.

Figure 5.12 emphasizes the flame height behavior of the two different calculations and the experiment of Aachen Surrogate. All three lines are linear curves with a coefficient of determination of $R^2 = 1$ for the calculations and $R^2 = 0.9767$ for the experiment to show differences and similarities between calculation and experiment best. We can see now that the gradient with the twenty five term calculation (Equation 4.8) is closer to the gradient of the experiment than the one of the small c calculation (Equation 5.1). The difference between the experiment gradient and the twenty five term calculation gradient is 3.85° and the small c calculation gradient is 6.46° . We also miss a zero offset for the trend lines of the calculations they have only zero flame height at zero fuel stream velocity. The linear trend line of the Aachen Surrogate flame height experiment has a zero offset of -35.696 mm .

Chapter 6.

Concluding Remarks

Previous research reveals that the flame heights and lift off hysteresis heights for liquid fuels are a relatively new field of study. The main focus of this diploma thesis was to find similarities between jet fuels and other surrogate fuels for the co-flow burner experiment. To compare this data to a numeric model numeric model, the Burke-Schumann equation was used.

A comparison for the flame height obtained from the jet fuels and surrogates shows a very good match between the FT Shell GTL, Aachen Surrogate, JP-8 Surrogate C, and SERDP Surrogate over a wide interval of fuel stream velocity. For the lift-off height experiments there is a good agreement between JP-8, Aachen Surrogate, JP-8 Surrogate C, and SERDP Surrogate over a wide interval of fuel stream velocity. However, for the the lift-off hysteresis experiments there was no significant match in flame height between any of the jet fuels and surrogates. There was only a slight match found between JP-8, Modified SERDP Surrogate, and Gasoline Surrogate C .

The conclusion of this studies is that there is a need to improve and develop surrogates for different jet fuels and different kind of experiments for the diffusion flame co-flow burner experiment.

Bibliography

- [1] BIELEVELD, T., FRASSOLDATI, A., CUOCI, A., FARAVELLI, T., RANZI, E., NIEMANN, U., AND SESHADRI, K. Experimental and kinetic modeling study of combustion of gasoline, its surrogates and components in laminar non-premixed flows. *The Combustion Institute* 32 (2009), 493–500.
- [2] BIRD, R. B., STEWART, W. E., AND LIGHTFOOT, E. N. *Transport Phenomena*, sixth printing ed. John Wiley & Sons, Inc., 1965.
- [3] GLASSMAN, I., AND YETTER, R. A. *Combustion*, fourth edition ed. Elsevier Inc., 2008.
- [4] HUMER, S. Experimental and kinetic modeling study of combustion of jp-8, its surrogates and reference components in laminar nonpremixed flows. *Proceedings of the Combustion Institute* 31 (2007), 393–400.
- [5] HUMER, S., NIEMANN, U., SEISER, R., SESHADRI, K., AND PUCHER, E. Combustion of jet fuels and its surrogates in laminar nonuniform flows. *Proceedings of the European Combustion Meeting* (2009).
- [6] HUMER, S., SESHADRI, K., AND SEISER, R. Combustion of jet fuels and its surrogates in laminar nonuniform flows. *5th US Combustion Meeting* (2007).
- [7] MKS INSTRUMENTS. <http://www.mksinst.com>, 2010.
- [8] MOSES, C. A. Comparative evaluation of semi-synthetic jet fuel. *U.S. Air Force Research Laboratories Contract F33415-02-D-2299 through Universal Technology Corporation* (2008).
- [9] NATIONAL INSTITUTE OF STANDARDS AND TECHNOLOGY. *NIST Chemistry WebBook*. <http://webbook.nist.gov/chemistry>, 2005.
- [10] OMEGA ENGINEERING, INC. <http://www.omega.com>, 2010.
- [11] PARKASH, S. *Petroleum Fuels Manufacturing Handbook*. M Graw Hill, 2010.
- [12] RANZI, E., FARAVELLI, T., FRASSOLDATI, A., AND GRANATA, S. Wide-range kinetic modeling study of the pyrolysis, partial oxidation, and combustion of heavy n-alkanes. *ICE* 44 (2005), 5170 – 5183.
- [13] SONO-TEK. <http://www.sono-tek.com>, 2010.

-
- [14] SPRINGER, O. P. D. H. *Skriptum zur Vorlesung Messtechnik*. Technische Universität Wien - Institut für Mechanik und Mechatronik Abteilung Maschinendynamik und Messtechnik&Aktorik, 2004.
 - [15] STEYNBERG, A., AND DRY, M. *Fischer-Tropsch Technology*. Elsevier, 2004.
 - [16] TELEDYNE ISCO. <http://www.isco.com>, 2010.
 - [17] TERRY, S. D., AND LYONS, K. M. Turbulent lifted flames in the hysteresis regime and the effects of coflow. *Journal of Energy Resources Technology* 128 (2006), 319–324.
 - [18] UNITED STATES - DEPARTMENT OF LABOR. <http://www.dol.gov>, 2010.
 - [19] WATLOW. <http://www.watlow.com>, 2010.
 - [20] WILLIAMS, F. A. *Combustion Theory*, second edition ed. The Benjamin/Cummings Publishing Company Inc., 1985.

List of Figures

1.1.	The appearance of gaseous fuel jet flames [3].	10
1.2.	Species variation through a diffusion flame at a fixed height above the fuel jet tube [3]	10
2.1.	Schematic illustration of the experimental setup. The figure shows the co-flow burner, the vaporizer and the air, fuel and nitrogen feed system. .	11
2.2.	Schematic illustration of the control and measurement setup and the wiring of the experimental setup.	12
2.3.	The experimental setup: 1, In-house air supply; 2, Exhaust system; 3, Pyrex glass tube; 4, Fuel nozzle; 5, Burner body; 6, Custom built co-flow air heat exchanger; 7, Nitrogen mass flow controller; 8, Cooling air mass flow controller; 9, Cooling air supply.	14
2.4.	The experimental setup: 10, Nitrogen gas cylinder; 11, Solid stage relays; 12, Watlow PID temperature controllers; 13, Ultra sonic broadband generator; 14, MKS mass flow controller power supply and control unit; 15, Syringe pump; 16, Fuel supply.	15
2.5.	Sectional view of a Sono-Tek AccuMist™Nozzle with the specific experimental setting [13].	16
2.6.	The Teledyne Isco Model 500D syringe pump [16].	17
2.7.	The experimental setup: 17, Vaporizer with insulation; 18, Co-flow air mass flow controller; 19, Cooling air dryer; 20, Ultra sonic nozzle; 21, Heated fuel line with insulation; 22, Heated co-flow air line with insulation; 23, Custom built co-flow air heat exchanger.	18
2.8.	MKS 1179, MKS 1579A, and MKS M100B mass flow controller [7].	18
2.9.	Omega Instruments Heating Tape [10].	19
2.10.	Watlow Series 93 PID temperature controller [19].	20
2.11.	Omega®Thermocouple K-Type [10].	21
2.12.	The experimental setup: 24, Cooling air intake; 25, Nitrogen carrier gas intake; 26, Heating tape; 27, Cooling air outlet; 28, Fuel intake; 29, Vaporizer. .	21

2.13.	Placement of the DSLR camera with macro lens for data acquisition. T_1 and T_2 are the temperatures of the fuel and the oxidizer duct, v_1 and v_2 are the velocities of the fuel stream and the oxidizer stream, $Y_{F,1}$ and $Y_{O_2,2}$ are the mass fractions of fuel and oxygen.	23
2.14.	Definition of the height measurements during the tests.	24
4.1.	A diffusion flame at the mouth of a tube in a duct for the underventilated and the overventilated case. Y_O is the mixture strenth of oxidizer and Y_F is the mixture strength of fuel [20].	30
4.2.	Flame shapes for the Burke-Schumann problem with $c = \frac{1}{2}$ [20].	32
4.3.	Sumfunction of Equation 4.6 with increasing ϕ_n	34
5.1.	Comparison of the flame height at constant fuel mass fraction $Y_{F,1} = 0.25$ as a function of the fuel stream velocity. The figure shows data for JP-8, FT IPK Sasol, and FT Shell GTL. The symbols represent experimental data and the lines are of polynomial second order best fit curves.	36
5.2.	Comparison of the flame height at constant fuel mass fraction $Y_{F,1} = 0.25$ as a function of the fuel stream velocity. The figure shows data for JP-8, Aachen Surrogate, SERDP Surrogate, JP-8 Surrogate C, Modified SERDP Surrogate, and Gasoline Surrogate C. The symbols represent experimental data and the lines are of polynomial second order best fit curves.	37
5.3.	Comparison of the flame height at constant fuel mass fraction $Y_{F,1} = 0.25$ as a function of the fuel stream velocity. The figure shows the data for FT IPK Sasol, Aachen Surrogate, SERDP Surrogate, JP-8 Surrogate C, and FT Shell GTL. The symbols represent experimental data and the lines are of polynomial second order best fit curves.	38
5.4.	Comparison of the lift-off height at constant fuel stream velocity $v_1 = 75 \text{ cm/s}$ as a function of the fuel mass fraction. The figure shows data for FT IPK Sasol, JP-8 and FT Shell. The symbols represent experimental data and the lines are of polynomial second order best fit curves.	40
5.5.	Comparison of the lift-off height at constant fuel stream velocity $v_1 = 75 \text{ cm/s}$ as a function of the fuel mass fraction. The figure shows data for Gasoline Surrogate C, JP-8, SERDP Surrogate, JP-8 Surrogate C, Aachen Surrogate, and Modified SERDP Surrogate. The symbols represent experimental data and the lines are of polynomial second order best fit curves.	41

5.6. Comparison of the flame height during lift-off height at constant fuel stream velocity $v_1 = 75 \text{ cm/s}$ as a function of the fuel mass fraction. The figure shows data for JP-8, FT Shell and FT IPK Sasol. The symbols represent experimental data and the lines are of polynomial second order best fit curves.	42
5.7. Comparison of the flame height during lift-off height at constant fuel stream velocity $v_1 = 75 \text{ cm/s}$ as a function of the fuel mass fraction. The figure shows data for JP-8, Modified SERDP Surrogate, JP-8 Surrogate C, SERDP Surrogate, Aachen Surrogate, and Gasoline Surrogate C. The symbols represent experimental data and the lines are of polynomial second order best fit curves.	43
5.8. Flame height for the diffusion flame problem by Burke-Schumann for JP-8, SERDP Surrogate, Aachen Surrogate, Modified SERDP Surrogate, JP-8 Surrogate C, and Gasoline Surrogate c as a function of the fuel stream velocity.	46
5.9. Flame height for the diffusion flame problem by Burke-Schumann for JP-8, FT IPK Sasol, and FT Shell GTL as a function of the fuel stream velocity.	47
5.10. Flame height for the diffusion flame problem by Burke-Schumann for pure n-Dodecane, n-Decane, iso-Octane, n-Heptane, Methylcyclohexane, Trimethylbenzene, and Toluene as a function of the fuel stream velocity.	47
5.11. Comparison flame height calculation for small c, flame height calculation with twenty five terms, and measured flame heights during the experiments as a function of fuel stream velocity v_1 of SERDP Surrogate, Aachen Surrogate, and JP-8 Surrogate C.	48
5.12. Comparison flame height calculation for small c, flame height calculation with twenty five terms, and measured flame heights during the experiments as a function of fuel stream velocity v_1 of Aachen Surrogate. The lines are linear best fit curves with coefficient of determination shown and linear equation.	49
A.1. Pictures of JP-8, FT Shell GTL, FT IPK Sasol, Aachen Surrogate, JP-8 Surrogate C, SERDP Surrogate, Modified SERDP Surrogate, and Gasoline Surrogate C flame at $\dot{V}_{F,1} = 0.150 \text{ ml/min}$ during the flame height experiment in the co-flow burner at $Y_{F,1} = 0.25$, and $T_1 = 480 \text{ K}$	vi
A.2. Pictures of JP-8, FT Shell GTL and FT IPK Sasol, Aachen Surrogate, JP-8 Surrogate C, SERDP Surrogate, Modified SERDP Surrogate, and Gasoline Surrogate C flame at $\dot{V}_{F,1} = 0.250 \text{ ml/min}$ during the flame height experiment in the co-flow burner at $Y_{F,1} = 0.25$, and $T_1 = 480 \text{ K}$	vii

A.3.	Pictures of JP-8, FT Shell GTL, FT IPK Sasol, Aachen Surrogate, JP-8 Surrogate C, SERDP Surrogate, Modified SERDP Surrogate, and Gasoline Surrogate C flame at $\dot{V}_{F,1} = 0.300ml/min$ during the flame height experiment in the co-flow burner at $Y_{F,1} = 0.25$, and $T_1 = 480K$	viii
A.4.	Pictures of JP-8, FT Shell GTL, FT IPK Sasol, Aachen Surrogate, JP-8 Surrogate C, SERDP Surrogate, Modified SERDP Surrogate, and Gasoline Surrogate C flame close to lift off conditions during the flame height experiment in the co-flow burner at $Y_{F,1} = 0.25$, and $T_1 = 480K$	ix
B.1.	Pictures of JP-8, FT Shell GTL, FT IPK Sasol, Aachen Surrogate, JP-8 Surrogate C, SERDP Surrogate, Modified SERDP Surrogate, and Gasoline Surrogate C flame close before lift off during the lift off hysteresis experiment in the co-flow burner at $v_1 = 75cm/s$, and $T_1 = 480K$	xv
B.2.	Pictures of JP-8, FT Shell GTL, FT IPK Sasol, Aachen Surrogate, JP-8 Surrogate C, SERDP Surrogate, Modified SERDP Surrogate, and Gasoline Surrogate C flame after lift off during the lift off hysteresis experiment in the co-flow burner at $v_1 = 75cm/s$, and $T_1 = 480K$	xvi
B.3.	Pictures of JP-8, FT Shell GTL, FT IPK Sasol, Aachen Surrogate, JP-8 Surrogate C, SERDP Surrogate, Modified SERDP Surrogate, and Gasoline Surrogate C flame close to the nozzle during the lift off hysteresis experiment in the co-flow burner at $v_1 = 75cm/s$, and $T_1 = 480K$	xvii
B.4.	Pictures of JP-8, FT Shell GTL, FT IPK Sasol, Aachen Surrogate, JP-8 Surrogate C, SERDP Surrogate, Modified SERDP Surrogate, and Gasoline Surrogate C flame returned to the nozzle during the lift off hysteresis experiment in the co-flow burner at $v_1 = 75cm/s$, and $T_1 = 480K$	xviii

List of Tables

1.1. Properties of Jet Fuels and Surrogates used during the Experiments	3
1.2. Aachen Surrogate composition and properties of employed components . .	6
1.3. JP-8 Surrogate C composition and properties of employed components . .	6
1.4. SERDP Surrogate composition and properties of employed components . .	7
1.5. Modified SERDP Surrogate composition and properties of employed components	7
1.6. Gasoline Surrogate C composition and properties of employed components	8
1.7. Properties of all single surrogate components in detail [9] [18].	8
3.1. t Distribution by William Sealy Gosset	27
4.1. φ_n , $J_0(\varphi_n)$, $J_1(c\varphi_n)$ and graph points for η of JP-8.	33
5.1. Burke-Schumann Problem for Fuels and Surrogates Calculation Data - η , ν , and diffusion coefficient at a fuel mass fraction $Y_{F,1} = 0.25$	44
5.2. Burke-Schumann Problem for Pure Hydrocarbons Calculation Data - η , ν , and diffusion coefficient at a fuel mass fraction $Y_{F,1} = 0.25$	45
5.3. Burke-Schumann Problem for Pure Hydrocarbons Calculation Data- η , ν , and diffusion coefficient at fuel mass fraction $Y_{F,1} = 0.4$ in comparison with experimental flame height data.	45
A.1. Experimental results of JP-8, FT Shell GTL, FT IPK Sasol, Aachen Surrogate, JP-8 Surrogate C, SERDP Surrogate, Modified SERDP Surrogate, and Gasoline Surrogate C for flame heights at constant fuel mass fraction $Y_{F,1} = 0.25$ and constant co-flow air velocity $v_2 = 47.6 \text{ cm/s}$	ii
B.1. Experimental results of JP-8, FT Shell GTL, FT IPK Sasol, Aachen Surrogate, JP-8 Surrogate C, SERDP Surrogate, Modified SERDP Surrogate, and Gasoline Surrogate C for lift off heights and flame heights during lift off hysteresis experiment at constant fuel stream velocity $v_1 = 75 \text{ cm/s}$ and constant co-flow air velocity $v_2 = 47.6 \text{ cm/s}$	xi

Appendix A.

A.1. Experimental Data for Flame Height Experiment

Detailed experimental data and pictures for the flame height experiment at constant fuel mass fraction ($Y_{F,1} = 0.25$).

Table A.1.: Experimental results of JP-8, FT Shell GTL, FT IPK Sasol, Aachen Surrogate, JP-8 Surrogate C, SERDP Surrogate, Modified SERDP Surrogate, and Gasoline Surrogate C for flame heights at constant fuel mass fraction $Y_{F,1} = 0.25$ and constant co-flow air velocity $v_2 = 47.6 \text{ cm/s}$

Fuel	Fuel Duct Temp. T_1 [K]	Fuel Flow Rate $\dot{V}_{F,1}$ [ml/min]	N_2 -Flow Rate $\dot{V}_{N_2,1}$ [Lpm]	Fuel Stream Velocity, v_1 [cm/s]	Flame Height \bar{z}_f [mm]	Standard Deviation \bar{s}_f [mm]
JP-8	480	0.150	0.289	28.231	10.9	0.6
		0.200	0.386	37.706	34.2	1.0
		0.250	0.482	47.084	51.4	0.9
		0.300	0.579	56.560	68.3	0.6
		0.330	0.636	62.128	79.4	0.5
		0.336	0.648	63.300	81.6	1.0
		0.338	0.652	63.691	82.5	1.0
		0.339	0.654	63.886	85.0	2.2
FT Shell GTL	480	0.150	0.289	25.887	7.9	0.3
		0.200	0.386	34.483	20.5	0.6
		0.250	0.482	43.177	37.6	1.4
		0.300	0.579	51.774	53.6	0.4
		0.330	0.636	69.064	81.0	0.9
		0.336	0.648	79.419	97.8	0.7
		0.338	0.652	81.079	100.4	1.3
		0.339	0.654	82.642	103.1	0.8

continued on next page...

Fuel	Fuel Duct Temp. T_1 [K]	Fuel Flow Rate $\dot{V}_{F,1}$ [ml/min]	N_2 -Flow Rate $\dot{V}_{N_2,1}$ [Lpm]	Fuel Stream Velocity, v_1 [cm/s]	Flame Height \bar{z}_f [mm]	Standard Deviation \bar{s}_f [mm]
FT IPK Sasol	480	0.150	0.289	26.961	9.2	0.2
		0.200	0.386	36.046	25.8	1.7
		0.250	0.482	45.033	45.1	0.9
		0.300	0.579	54.020	59.9	0.7
		0.330	0.636	63.007	74.7	0.7
		0.336	0.648	64.863	77.3	0.8
		0.338	0.652	65.742	79.3	0.2
		0.339	0.654	66.621	80.4	0.6
		0.150	0.272	28.375	8.4	0.25
		0.200	0.362	37.768	26.1	1.6
Aachen Surrogate	480	0.250	0.453	47.259	45.7	1.7
		0.300	0.544	56.750	59.9	1.0
		0.350	0.634	66.143	75.9	0.8
		0.400	0.725	75.634	92.6	0.6
		0.408	0.739	77.098	95.3	1.2
		0.412	0.747	77.928	96.2	0.4

continued on next page...

Fuel	Fuel Duct Temp. T_1 [K]	Fuel Flow Rate $\dot{V}_{F,1}$ [ml/min]	N_2 -Flow Rate $\dot{V}_{N_2,1}$ [Lpm]	Fuel Stream Velocity, v_1 [cm/s]	Flame Height \bar{z}_f [mm]	Standard Deviation \bar{s}_f [mm]
JP-8	480	0.150	0.278	29.076	9.4	0.1
Surrogate C		0.200	0.371	38.801	30.1	0.4
		0.250	0.464	48.526	46.7	0.3
		0.300	0.557	58.251	62.2	0.3
		0.350	0.650	67.975	79.7	0.2
		0.375	0.696	72.789	87.4	1.0
		0.390	0.724	75.716	92.8	0.4
		0.405	0.752	78.643	97.5	0.6
SERDP	480	0.150	0.269	27.853	8.9	0.5
Surrogate		0.200	0.359	37.170	26.2	1.1
		0.250	0.449	46.487	44.2	0.8
		0.300	0.538	55.707	60.0	0.6
		0.350	0.628	65.024	74.8	1.1
		0.400	0.718	74.341	91.4	0.9
		0.430	0.772	78.999	97.6	0.5

continued on next page...

Fuel	Fuel Duct Temp. T_1 [K]	Fuel Flow Rate $\dot{V}_{F,1}$ [ml/min]	N_2 -Flow Rate $\dot{V}_{N_2,1}$ [Lpm]	Fuel Stream Velocity, v_1 [cm/s]	Flame Height \bar{z}_f [mm]	Standard Deviation \bar{s}_f [mm]
Modified SERDP Surrogate	480	0.150	0.277	28.795	8.3	0.2
		0.200	0.370	38.458	25.5	0.9
		0.250	0.462	48.024	44.0	0.5
		0.300	0.555	57.687	60.2	0.6
		0.350	0.647	67.253	74.6	0.7
		0.400	0.740	76.916	91.5	0.5
		0.420	0.777	80.762	97.1	0.6
		0.422	0.781	81.176	98.8	1.1
Gasoline Surrogate C	480	0.150	0.268	28.540	8.6	0.5
		0.200	0.357	38.021	21.2	0.2
		0.250	0.446	47.502	41.3	0.3
		0.300	0.535	56.983	55.7	0.5
		0.350	0.624	66.464	69.7	0.6
		0.400	0.713	75.945	85.2	1.3
		0.420	0.749	79.776	90.9	1.4
		0.423	0.754	80.312	91.6	0.9

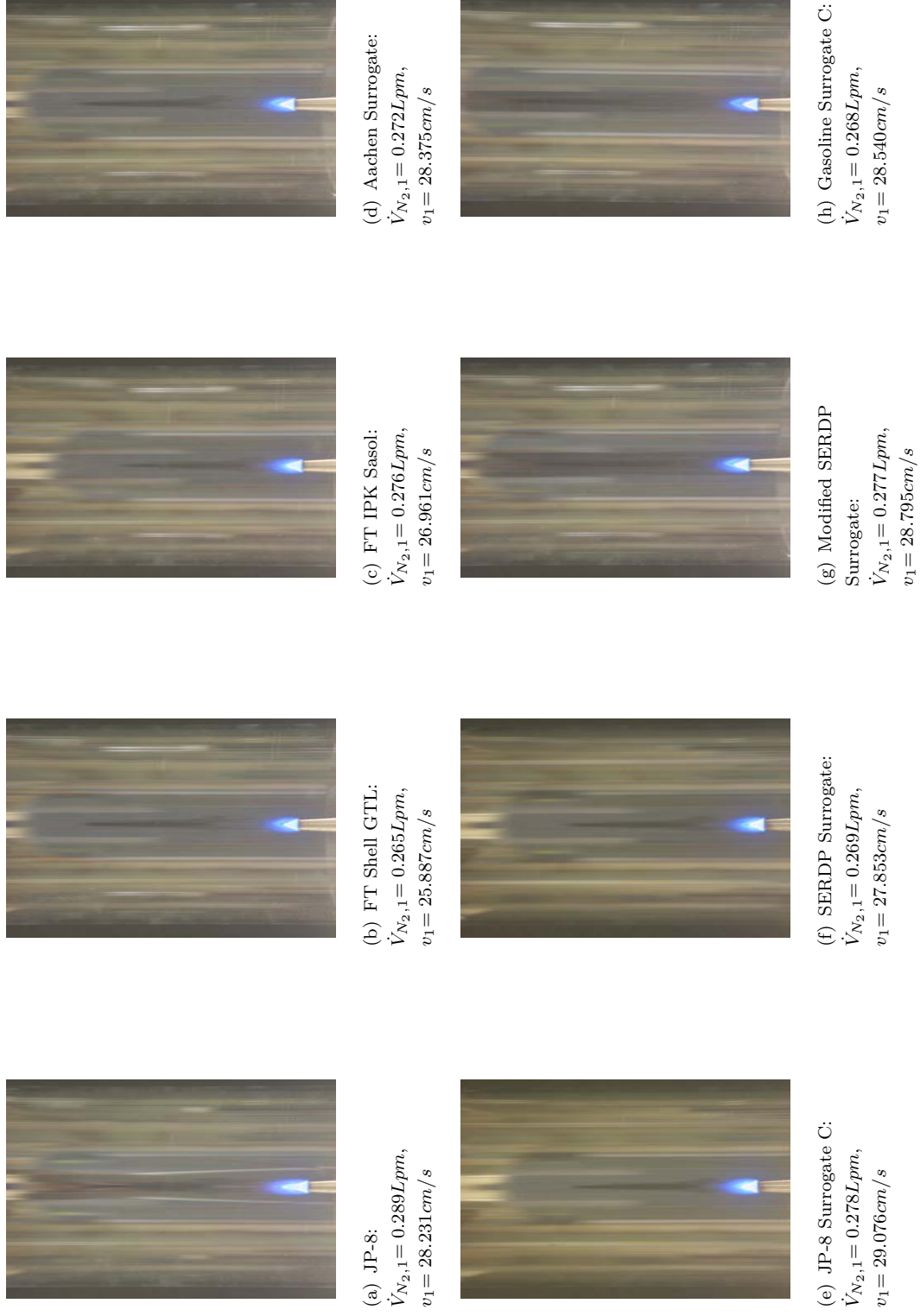


Figure A.1.: Pictures of JP-8, FT Shell GTL, FT IPK Sasol, Aachen Surrogate, JP-8 Surrogate C, SERDP Surrogate, Modified SERDP Surrogate, and Gasoline Surrogate C flame at $\dot{V}_{F,1} = 0.150 ml/min$ during the flame height experiment in the co-flow burner at $Y_{F,1} = 0.25$, and $T_1 = 480K$.

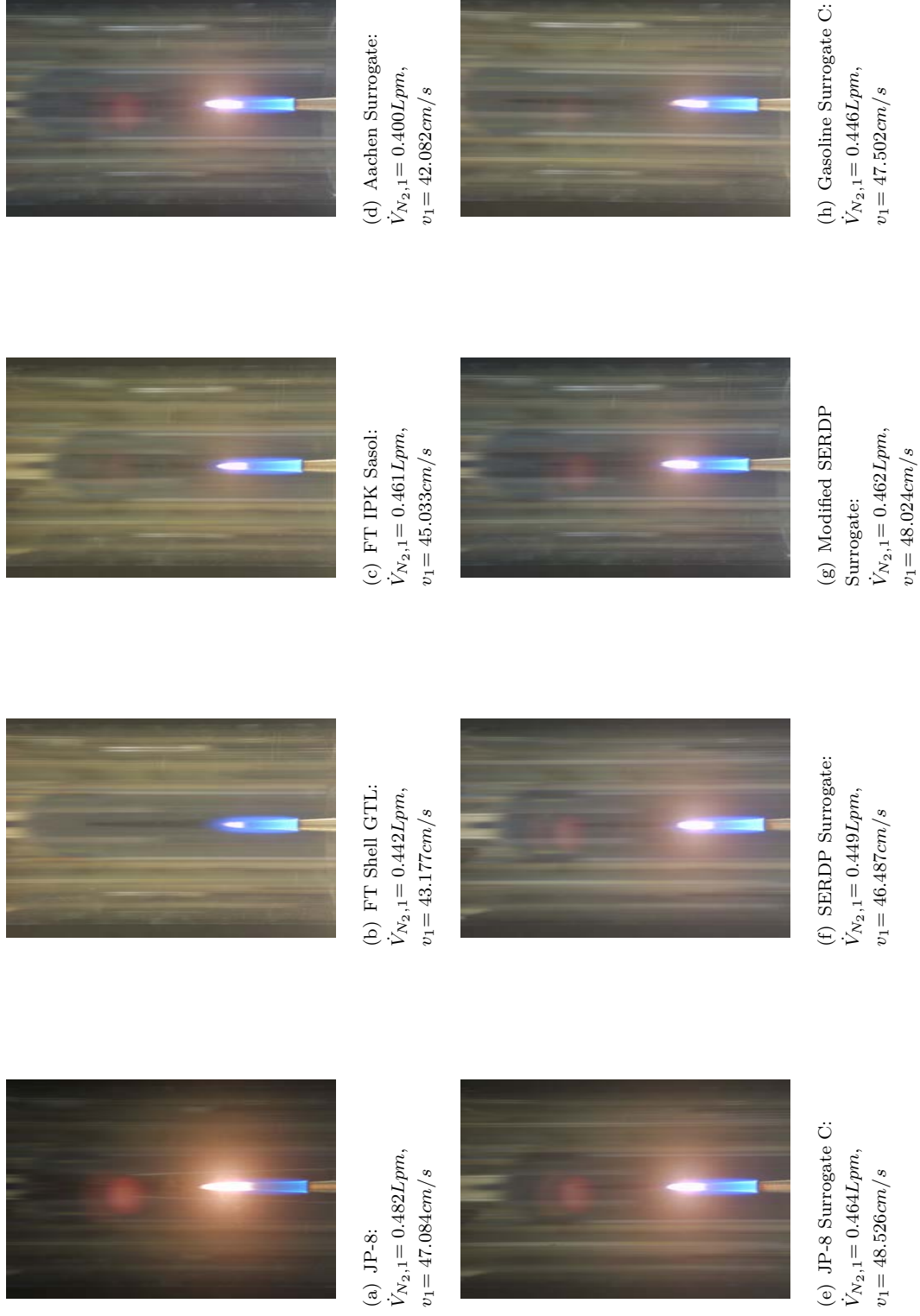


Figure A.2.: Pictures of JP-8, FT Shell GTL and FT IPK Sasol, Aachen Surrogate, JP-8 Surrogate C, SERDP Surrogate, Modified SERDP Surrogate, and Gasoline Surrogate C flame at $\dot{V}_{F,1} = 0.250 ml/min$ during the flame height experiment in the co-flow burner at $Y_{F,1} = 0.25$, and $T_1 = 480K$.

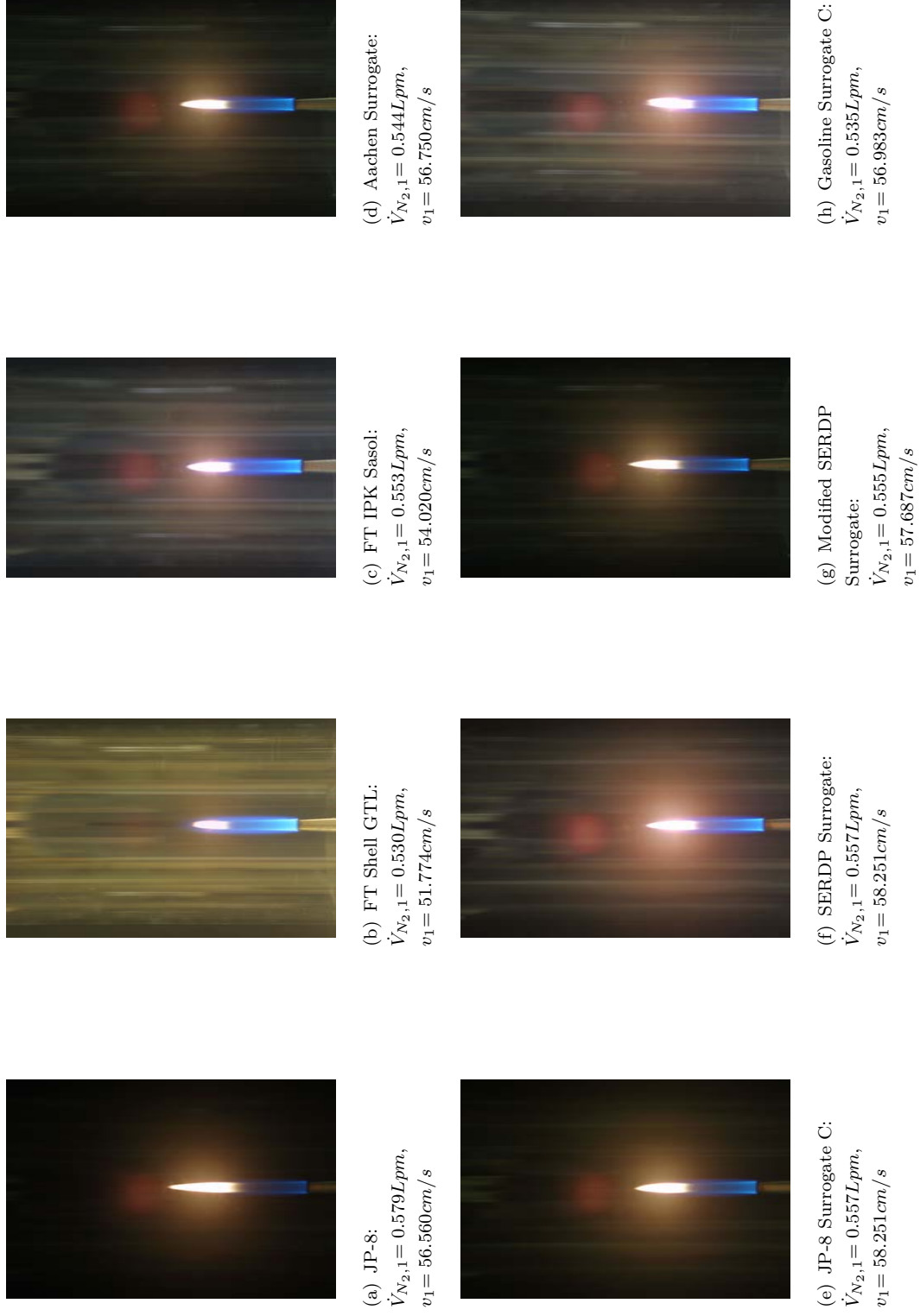


Figure A.3.: Pictures of JP-8, FT Shell GTL, FT IPK Sasol, Aachen Surrogate, JP-8 Surrogate, SERDP Surrogate, Modified SERDP Surrogate, and Gasoline Surrogate C flame at $\dot{V}_{F,1} = 0.300 ml/min$ during the flame height experiment in the co-flow burner at $Y_{F,1} = 0.25$, and $T_1 = 480K$.

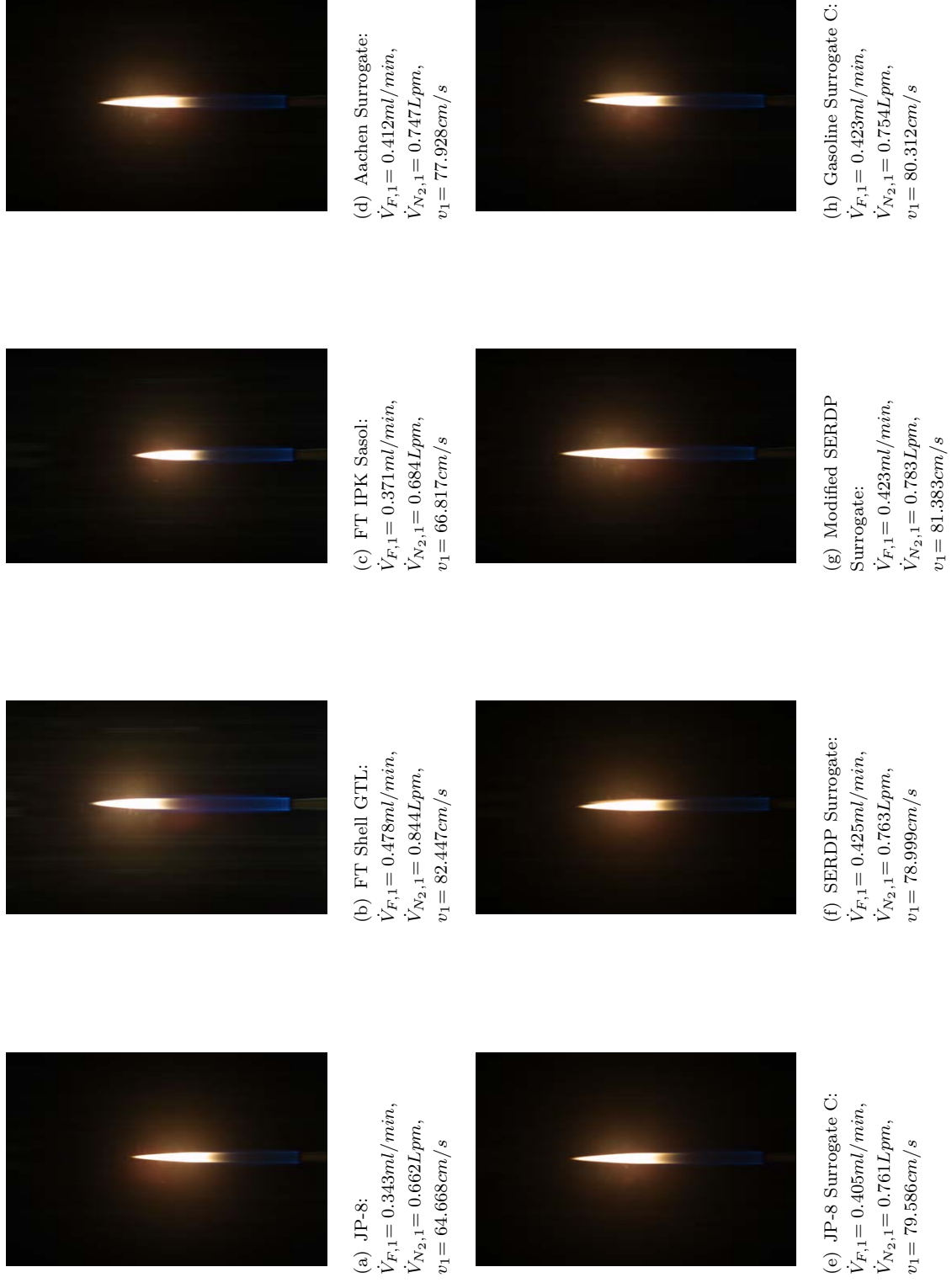


Figure A.4.: Pictures of JP-8, FT Shell GTL, FT IPK Sasol, Aachen Surrogate, JP-8 Surrogate, Modified SERDP Surrogate, and Gasoline Surrogate C flame close to lift off conditions during the flame height experiment in the co-flow burner at $Y_{F,1} = 0.25$, and $T_1 = 480 \text{ K}$.

Appendix B.

B.1. Experimental Data for Lift-Off Height Hysteresis Experiment

Detailed experimental data and pictures for the lift off height hysteresis and flame height during lift off hysteresis experiment at constant fuel stream velocity ($v_1 = 75 \text{ cm/s}$).

Fuel	Fuel Line Temp. T_1 [K]	Fuel Flow Rate $\dot{V}_{F,1}$ [ml/min]	N_2 -Flow Rate $\dot{V}_{N_2,1}$ [Lpm]	Fuel Mass Fraction $Y_{F,1}$ [-]	Lift Off Height $\bar{z}_{lift-off}$ [mm]	Stand.Deviation Lift Off $\bar{s}_{lift-off}$ [mm]	Flame Height \bar{z}_f [mm]	Stand.Deviation Flame Height \bar{s}_f [mm]
FT IPK Sasol	480	0.414	0.726	0.259	0	0	97.0	0.9
		0.394	0.728	0.250	186.5	3.1	30.1	0.6
		0.434	0.724	0.269	169.4	4.5	40.9	2.3
		0.473	0.720	0.288	158.6	4.0	51.0	2.8
		0.513	0.716	0.306	141.9	3.2	66.5	2.7
		0.552	0.712	0.323	121.6	6.2	81.6	4.0
		0.592	0.708	0.339	103.0	1.8	101.2	4.6
Aachen Surrogate	480	0.632	0.704	0.355	0	0	160.6	1.3
		0.404	0.718	0.254	0	0	88.8	2.5
		0.372	0.722	0.237	182.3	1.2	20.5	0.6
		0.420	0.716	0.262	161.4	1.3	35.9	0.6
		0.453	0.712	0.278	141.2	2.3	49.7	0.7
		0.485	0.708	0.293	126.9	3.2	59.5	1.8
		0.518	0.704	0.308	113.6	2.4	74.3	1.4
		0.550	0.700	0.322	103.0	5.3	86.9	2.0
		0.566	0.698	0.329	0	0	138.6	1.8

continued on next page...

Fuel	Fuel Line Temp. T_1 [K]	Fuel Flow Rate $\dot{V}_{F,1}$ [ml/min]	N_2 -Flow Rate $\dot{V}_{N_2,1}$ [Lpm]	Fuel Mass Fraction $Y_{F,1}$ [-]	Lift Off Height $\bar{z}_{lift-off}$ [mm]	Stand.Deviation Lift Off $\bar{s}_{lift-off}$ [mm]	Flame Height \bar{z}_f [mm]	Stand.Deviation Flame Height \bar{s}_f [mm]
JP-8	480	0.395	0.716	0.255	0	0	92.0	0.7
Surrogate C		0.365	0.720	0.239	190.2	1.7	19.1	0.2
		0.426	0.712	0.270	157.2	2.1	42.1	0.8
		0.456	0.708	0.285	140.5	2.5	52.6	1.0
		0.487	0.704	0.300	121.8	3.3	69.9	1.3
		0.517	0.700	0.314	105.2	4.4	84.4	2.0
		0.548	0.696	0.327	93.9	3.6	95.0	1.3
		0.578	0.692	0.341	0	0	147.2	2.9
SERDP	480	0.388	0.726	0.242	0	0	87.9	0.3
Surrogate		0.351	0.730	0.223	196.6	1.0	13.9	0.8
		0.426	0.722	0.242	161.4	0.8	41.2	0.4
		0.463	0.718	0.261	141.8	1.0	55.0	1.4
		0.500	0.714	0.278	122.1	3.8	70.4	1.4
		0.537	0.710	0.295	105.6	3.2	87.8	1.4
		0.574	0.706	0.311	85.6	2.7	107.1	1.7
		0.611	0.702	0.342	0	0	152.8	2.7

continued on next page...

Fuel	Fuel Line Temp. T_1 [K]	Fuel Flow Rate $\dot{V}_{F,1}$ [ml/min]	N_2 -Flow Rate $\dot{V}_{N_2,1}$ [Lpm]	Fuel Mass Fraction $Y_{F,1}$ [-]	Lift Off Height $\bar{z}_{lift-off}$ [mm]	Stand.Deviation Lift Off $\bar{s}_{lift-off}$ [mm]	Flame Height \bar{z}_f [mm]	Stand.Deviation Flame Height \bar{s}_f [mm]
Modified SERDP Surrogate	480	0.386 0.353 0.403 0.437 0.471 0.504 0.538 0.572	0.722 0.726 0.720 0.716 0.712 0.708 0.704 0.700	0.248 0.230 0.257 0.273 0.290 0.305 0.320 0.335	0 175.1 154.3 147.6 128.0 107.4 90.6 0	0 3.4 2.8 1.8 2.8 1.9 5.1 0	89.9 22.1 37.1 45.8 58.9 76.5 92.2 139.3	0.3 1.6 1.0 1.1 1.2 0.6 2.6 3.4
Gasoline Surrogate C	480	0.396 0.371 0.421 0.445 0.470 0.495 0.520 0.545	0.704 0.708 0.700 0.696 0.692 0.688 0.684 0.680	0.251 0.238 0.263 0.276 0.288 0.300 0.311 0.323	0 204.5 174.8 159.9 145.5 128.0 113.4 0	0 1.1 2.0 3.3 1.4 4.1 4.3 0	82.7 4.4 23.2 32.3 41.7 53.3 63.9 125.4	1.5 0.3 1.1 1.3 1.2 2.4 1.4 1.1

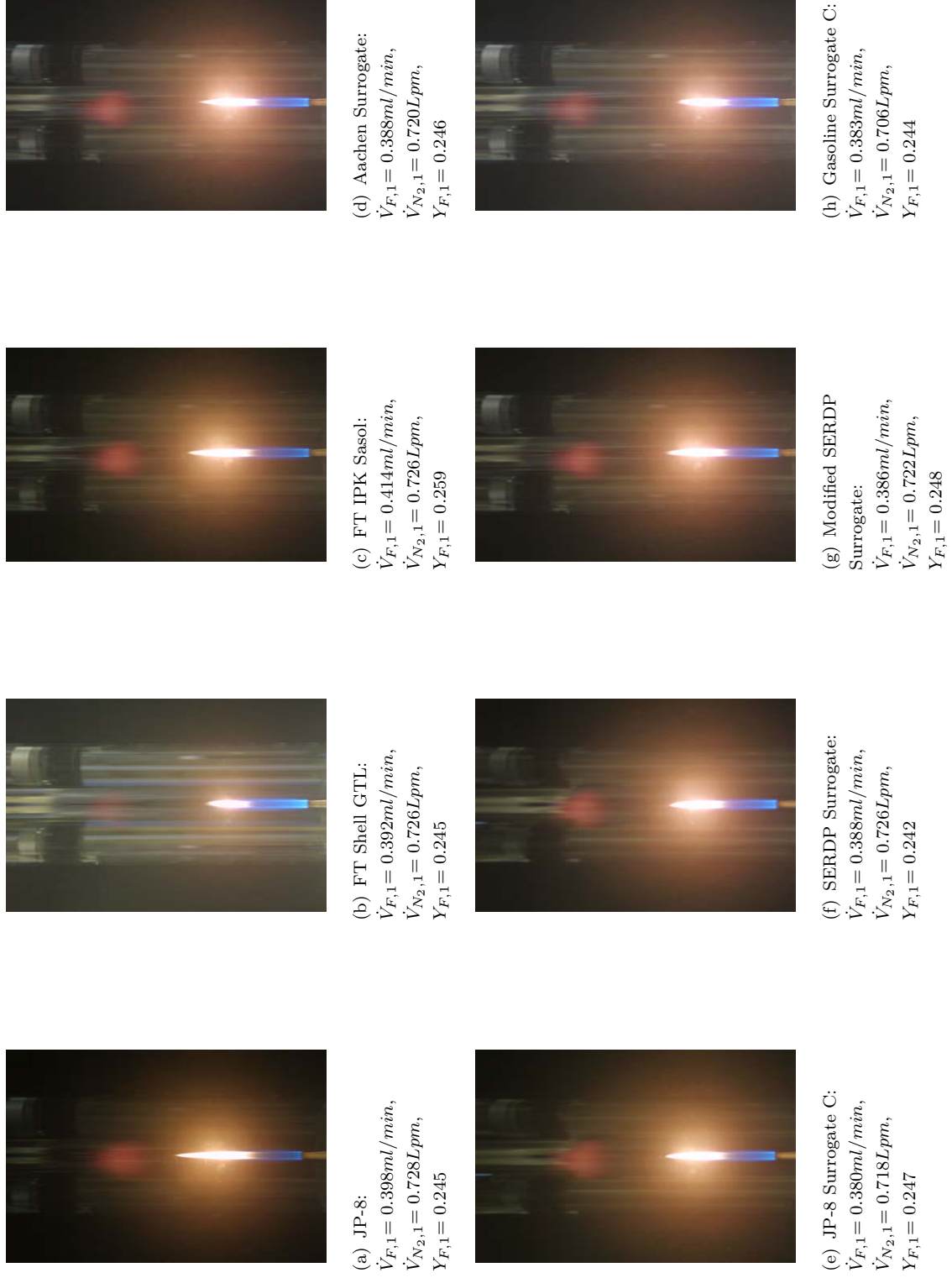


Figure B.1.: Pictures of JP-8, FT Shell GTL, FT IPK Sasol, Aachen Surrogate, JP-8 Surrogate C, SERDP Surrogate, Modified SERDP Surrogate, and Gasoline Surrogate C flame close before lift off during the lift off hysteresis experiment in the co-flow burner at $v_1 = 75 \text{ cm/s}$, and $T_1 = 480 \text{ K}$.

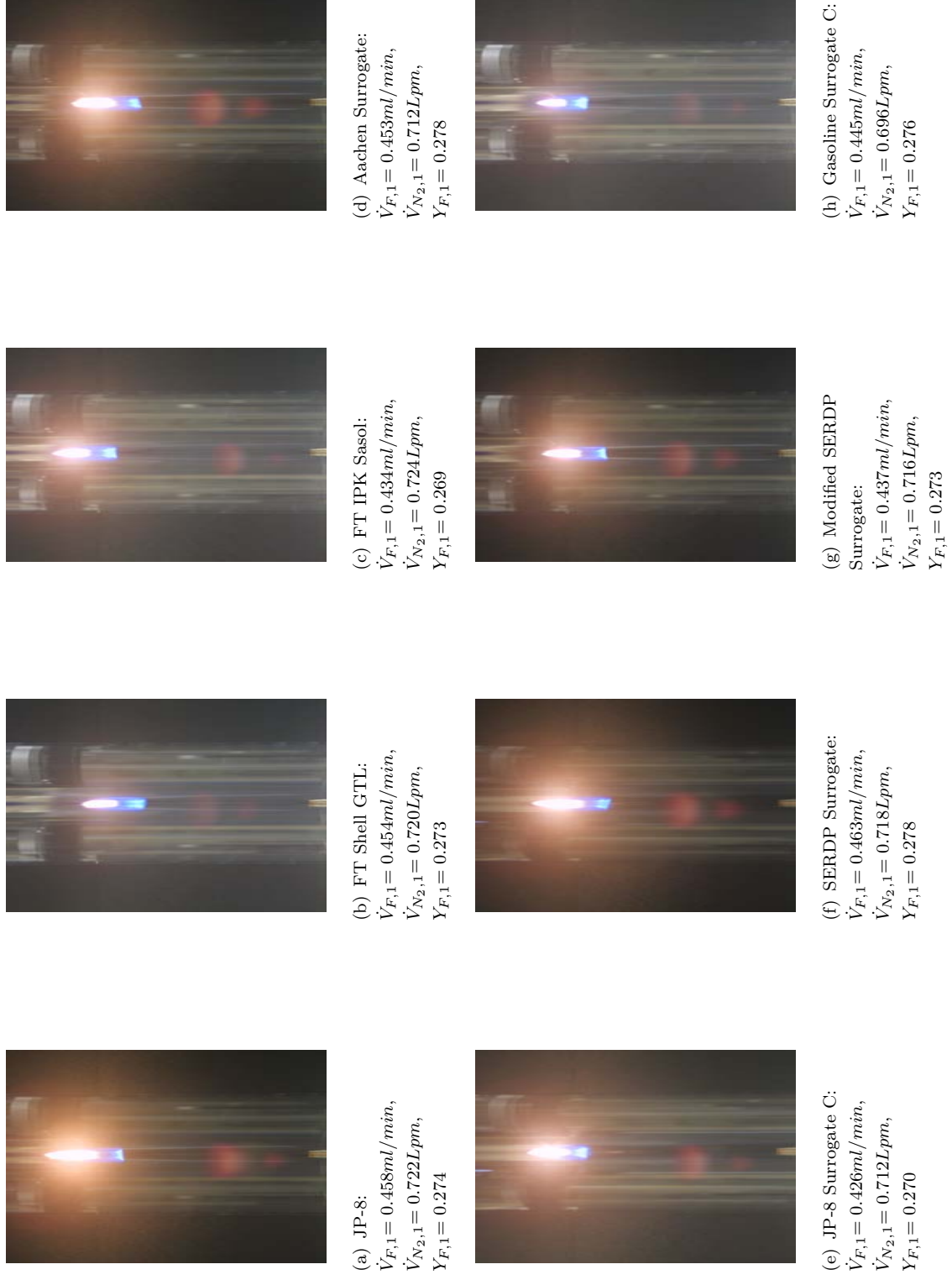


Figure B.2.: Pictures of JP-8, FT Shell GTL, FT IPK Sasol, Aachen Surrogate, JP-8 Surrogate C, SERDP Surrogate, Modified SERDP Surrogate, and Gasoline Surrogate C flame after lift off during the lift off hysteresis experiment in the co-flow burner at $v_1 = 75 \text{ cm/s}$, and $T_1 = 480 \text{ K}$.

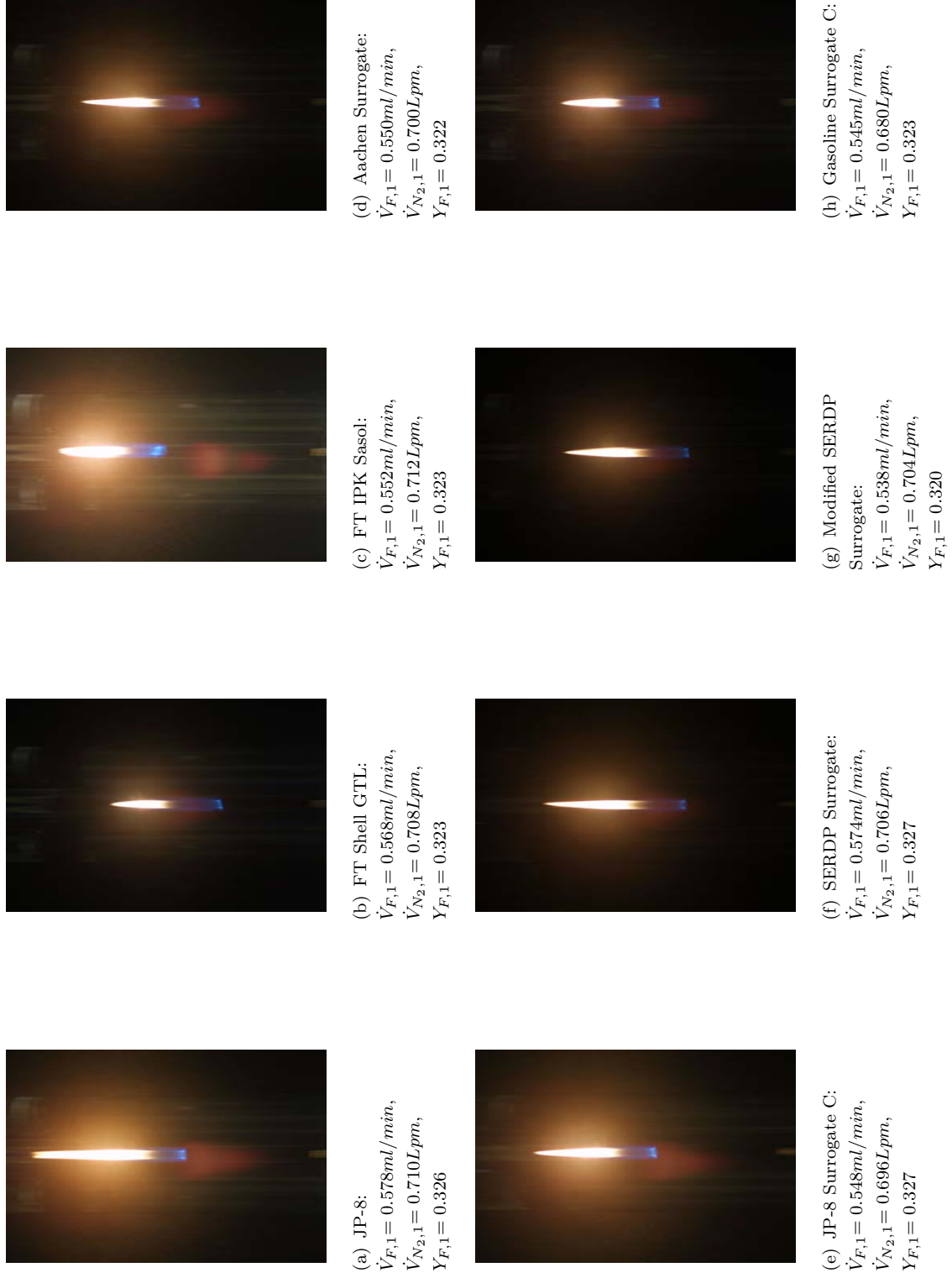


Figure B.3.: Pictures of JP-8, FT Shell GTL, FT IPK Sasol, Aachen Surrogate, JP-8 Surrogate C, SERDP Surrogate, Modified SERDP Surrogate, and Gasoline Surrogate C flame close to the nozzle during the lift off hysteresis experiment in the co-flow burner at $v_1 = 75 \text{ cm/s}$, and $T_1 = 480 \text{ K}$.

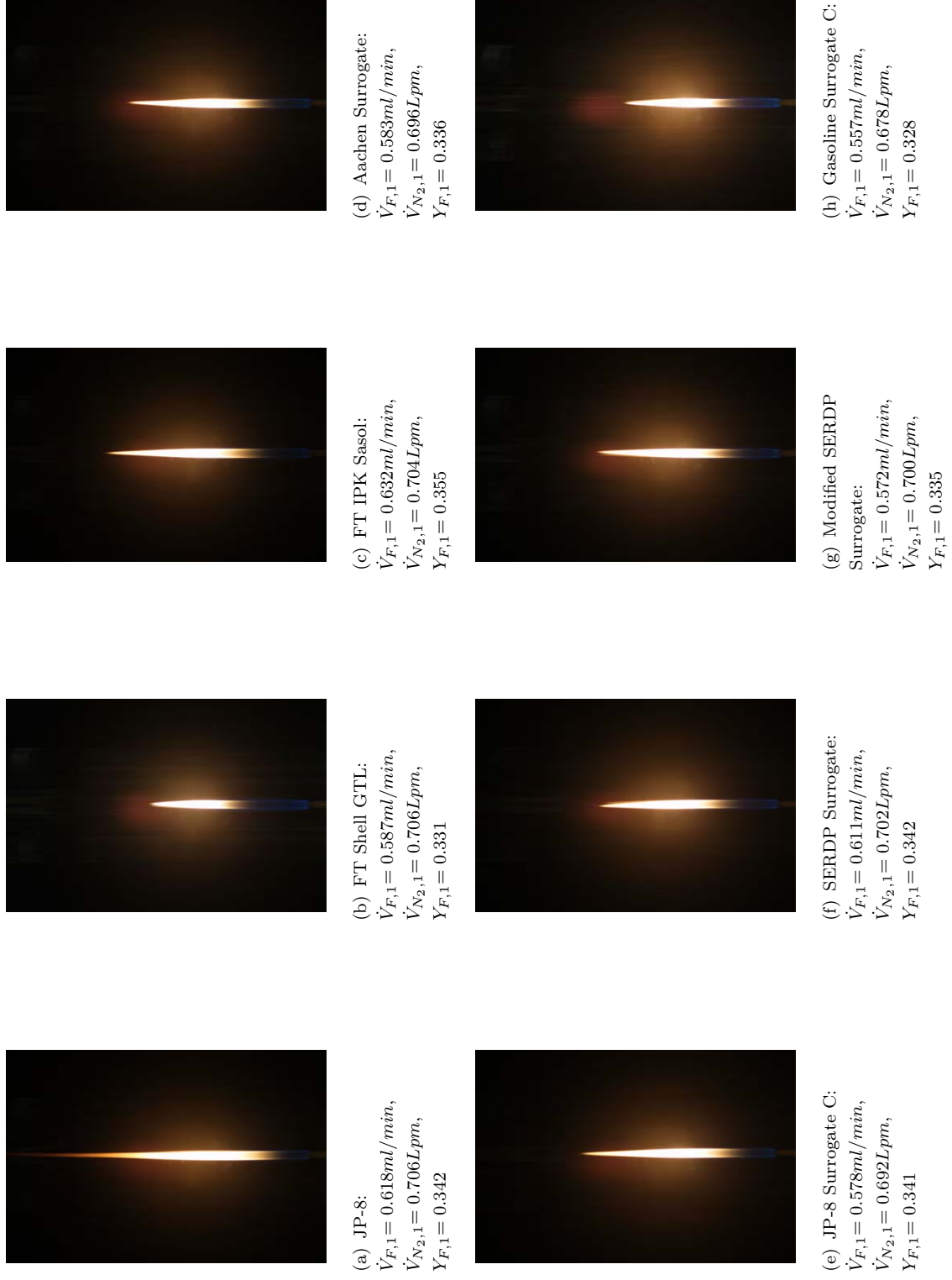


Figure B.4.: Pictures of JP-8, FT Shell GTL, FT IPK Sasol, Aachen Surrogate, JP-8 Surrogate C, SERDP Surrogate, Modified SERDP Surrogate, and Gasoline Surrogate C flame returned to the nozzle during the lift off hysteresis experiment in the co-flow burner at $v_1 = 75 \text{ cm/s}$, and $T_1 = 480 \text{ K}$.